Design and optimization of an intermediate heat exchanger in the Eskom advanced high temperature reactor

AJ Viljoen

orcid.org/0000-0003-4255-8048

Dissertation submitted in partial fulfilment of the requirements for the degree Master of Engineering in Nuclear Engineering at the North-West University

Supervisor: Dr AC Cilliers

Graduation ceremony May 2019

Student number: 24102199

ABSTRACT

The Eskom AHTR forms part of the next generation of nuclear reactors and aims to have a load following capability by storing heat in molten salt. The heat generated in the reactor is removed by Helium gas and should be transferred to the molten salt storage through an intermediate heat exchanger. A design is required for the intermediate heat exchanger that would successfully deliver the heat duty required. From the literature a printed circuit heat exchanger is chosen due to its high compactness and ability to handle high pressure differentials in the fluids. The material that the heat exchanger will consist off is chosen to be Hastelloy N due to its high resistance against corrosion and acceptable design stress at the operating conditions. A Flownex model is used to design and optimize the heat exchanger and to ensure that it matches the design specifications of the AHTR reactor. The results from the Flownex model are compared to an ANSYS Fluent simulation in order to verify the results. The two simulation programs delivered similar results and the model can be seen as a good representation of the actual heat exchanger. The final heat exchanger design can successfully deliver the heat duty required.

Key Words: Compact heat exchanger, Advanced High Temperature Reactor, Design, Helium, Molten Salt

DECLARATION

I, **AJ Viljoen**, declare that this report is a presentation of my own original work.

Whenever contributions of others are involved, every effort was made to indicate this clearly, with due reference to the literature.

No part of this work has been submitted in the past, or is being submitted, for a degree or examination at any other university or course.

Signed on the 20th day of November 2018, in Potchefstroom.

____

TABLE OF CONTENTS

LIST OF FIGURES

LIST OF TABLES

NOMENCLATURE

°C	Degree Celsius
μ	Viscosity
μm	Micrometre
AHTR	Advanced high temperature reactor
ASME	The American Society of Mechanical Engineers
Cp	Specific Heat
ε	Effectiveness
IHX	Intermediate heat exchanger
K	Kelvin
Kg/s	Kilogram per second
kPa	Kilopascal
MPa	Mega Pascal
MW	Megawatt
NTU	Number of transfer units
PCHE	Printed circuit heat exchanger
ρ	Density

1. INTRODUCTION

Advanced high temperature reactors (AHTR's) form part of the next generation of nuclear power plants and are designed to meet the demands of the future power grid. These reactors operate at high outlet temperatures where the heat generated can be used for electricity generation or several other chemical processes. To operate the AHTR, compact heat exchangers should be used to remove heat from the reactor core and transfer heat to the required processes.

AHTR REACTOR DESIGN

The AHTR is designed into several segments as shown in Figure 1. The power source cycle also known as the primary cycle consists of the reactor core with a turbine, low pressure compressor and a high pressure compressor where Helium is the working fluid. The battery component of the AHTR consists of two molten salt storage tanks that would be storing the heat generated in the primary cycle. The stored heat can then be transferred to a Rankine cycle where electricity is generated. The installation of the Rankine cycle for electricity generation is optional, and the heat in the molten salt storage can be used for several processes depending on the demand. The significance of the molten salt storage is that the AHTR can load follow the electricity demand without changing the power output of the primary cycle, therefore making load following possible at a higher efficiency.

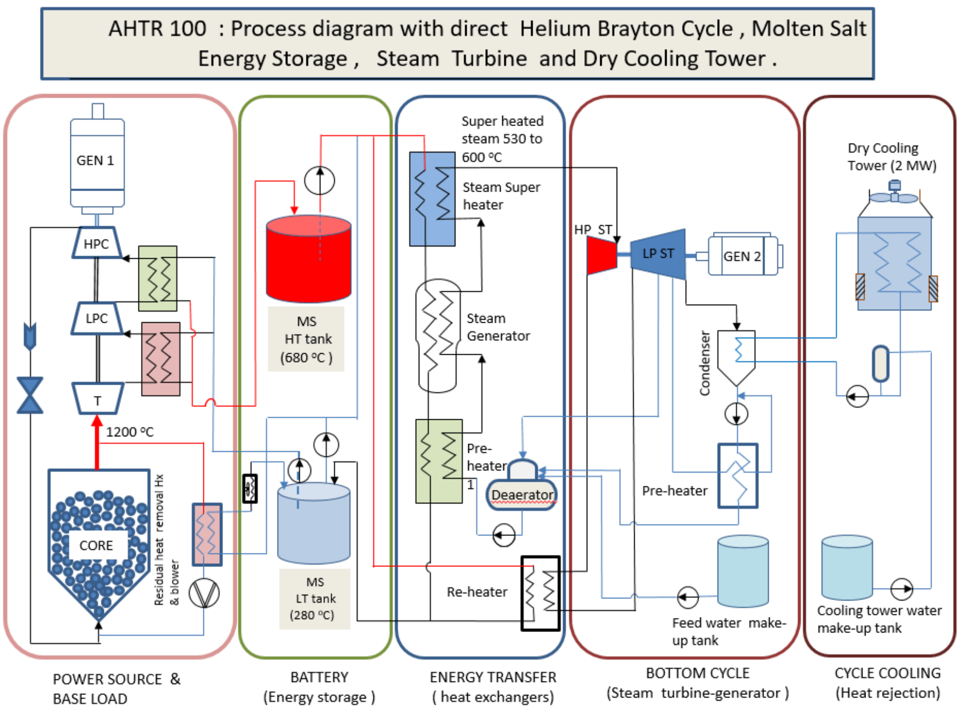

Figure 1: AHTR Process Diagram

THERMODYNAMIC CYCLES

The AHTR is designed to deliver a power output of 100 MW thermal energy. The Primary cycle will consist of a Helium Brayton cycle consisting of a high temperature turbine and several compressors to ensure a pressure of 9 MPa through the reactor core. The reactor core has a maximum inlet temperature of 400°C and a maximum outlet temperature of 1200°C.

The physical design of a reactor is done is such a way that it delivers 100MW of thermal energy at a specific reactor cycle efficiency. When the thermal energy output of the reactor is varied it then operates outside of the design conditions and has an effect on the cycle efficiency of the reactor. In order to maintain a high efficiency, it is advised to operate the reactor core at the design power level. The amount of heat that has to be removed from the core therefore should be constant during operation.

The heat generated in the reactor core is firstly transferred to a molten salt storage tank with the intermediate heat exchangers (IHX's). The molten salt storage will be able to provide heat during times of high demand and can be used as heat sink after reactor shutdown. During operation the molten salt storage tank is used as a heat source to power a Rankine cycle or any other chemical process where heat is required. The IHX's will be subjected to a unique set of conditions as heat will be transferred from high pressurized helium to an atmospheric pressured molten salt.(Storm 2017)

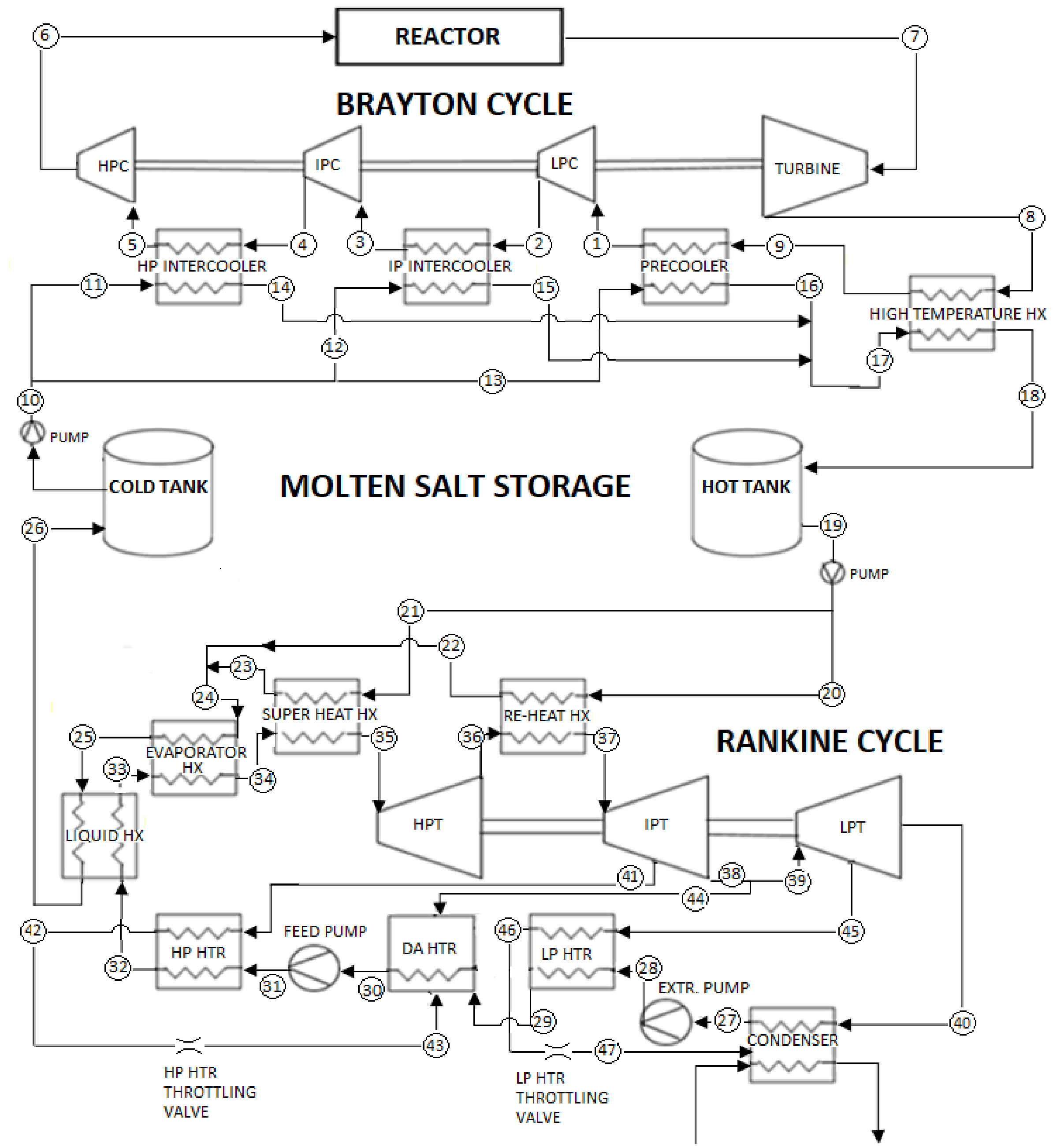

Figure 2: Brayton Cycle integrated with Molten Salt Storage

Table 1: Brayton Cycle

TOPPING BRAYTON CYCLE					
Point on Diagram	T_{He}	P_{He}	h_{He}	$\dot{m}_{He}$	**Working Fluid**
	[°C]	[kPa]	[kJ/kg]	[kg/s]	
1	338,413	2322,472	3188,423	24,092	Helium
2	510,766	4130,535	4088,761	24,092	Helium
3	338,413	4089,229	3193,988	24,092	Helium
4	510,355	7272,727	4096,187	24,092	Helium
5	338,413	7200,000	3203,756	24,092	Helium
6	400,000	9000,000	3528,905	24,092	Helium
7	1200,000	8920,000	7679,726	24,092	Helium
8	630,000	2369,154	4702,433	24,092	Helium
9	510,766	2345,697	4083,317	24,092	Helium

Table 2: Molten Salt Storage

MOLTEN SALT STORAGE					
Point on Diagram	**T_{MS}** [°C]	**P_{MS}** [kPa]	**h_{MS}** [kJ/kg]	**$\dot{m}_{MS}$** [kg/s]	**Working Fluid**
10	318,413	-	886,024	244,765	Solar Salt
11	318,413	-	886,024	81,582	Solar Salt
12	318,413	-	886,024	81,586	Solar Salt
13	318,413	-	886,024	81,597	Solar Salt
14	480,355	-	1149,562	81,582	Solar Salt
15	480,766	-	1150,243	81,586	Solar Salt
16	480,766	-	1150,243	81,597	Solar Salt
17	480,629	-	1150,016	244,765	Solar Salt
18	517,303	-	1210,955	244,765	Solar Salt
19	517,143	-	1210,689	244,765	Solar Salt
20	517,143	-	1210,689	91,904	Solar Salt
21	517,143	-	1210,689	152,861	Solar Salt
22	432,837	-	1071,299	91,904	Solar Salt
23	432,837	-	1071,299	152,861	Solar Salt
24	432,837	-	1071,299	244,765	Solar Salt
25	371,091	-	977,602	244,765	Solar Salt
26	318,413	-	886,024	244,765	Solar Salt

REACTOR ASSEBLY

In the initial design for the AHTR reactor there has been a specific allocated volume for the heat exchanger and pre-cooler units. For this study, the allocated volume will be used as a reference to the shape and size that the heat exchanging unit can be. The initial design can be seen in below in Figure 3. (Fox 2017)

From the 3D layout we can see that the reactor core is located at the bottom of the assembly with the power generation unit located at the top. The heat exchanger and pre-coolers are situated in the power generation unit and is illustrated by the red cylindrical components.

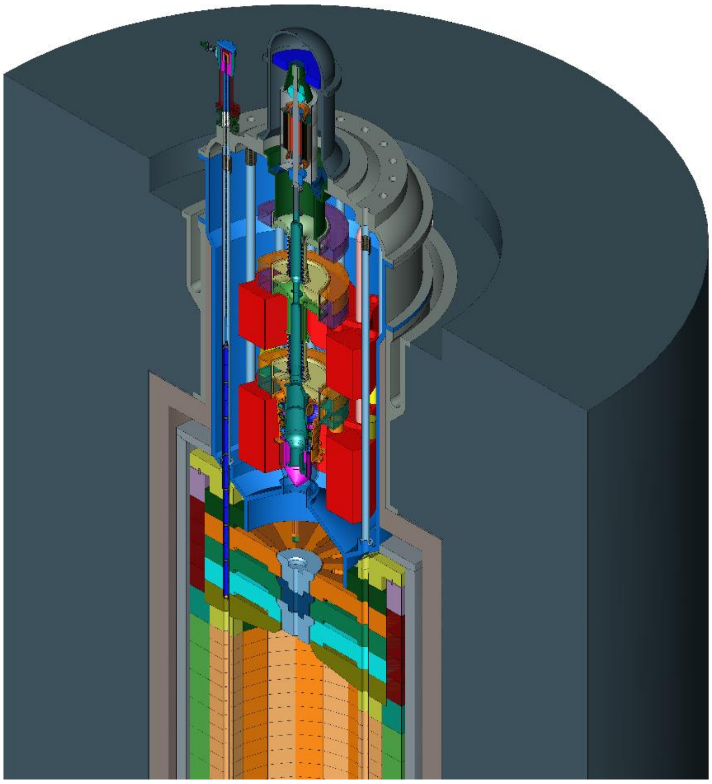

Figure 3: AHTR 3D power generation unit layout

INTERMEDIATE HIGH TEMPERATURE HEAT EXCHANGER

From the thermodynamic cycle design and physical reactor design the conditions and requirements for the IHX can be summed up in Table 3.

Table 3: IHX requirements and operating conditions

Parameter	Value
Operating Pressure	2369,154 kPa
Maximum Pressure in case of turbine failure	9000 kPa
Operating Temperature Ranges Helium	510.8 – 630 °C
Operating Temperature Ranges Molten Salt	480,6 - 517,3 °C
Maximum Temperature in case of a turbine failure.	1200 °C
Heat Duty	14908 kW
Effectiveness	0.7892
Estimated Power Density	12633 kW/m^3
Desired Pressure Drop in the Helium	23.5 kPa

Requirements Discussion

The operating temperature range of the helium falls within the range of other existing High Temperature Gas Reactors (HTGR), however the fluids used in these design are different(Chen, Sun et al. 2016).The AHTR requires heat to be transferred from high pressure helium to atmospheric pressure molten salt where other HTGR's either have a helium-to-steam or a helium-to-sCO2 configuration with both streams being under a high pressure (Aquaro and Pieve 2007). Concentrated Solar Power Plants use a similar fluid configuration for power generation with a salt-to-steam or a salt-to-sCO2 design, however the power density of these heat exchangers are much lower as they are not designed to fit into a modular nuclear reactors (Pizzolato, Donato et al. 2017). The lower power density completely changes the heat exchanger selection process (Hesselgreaves, Law et al. 2016).

Due to the large pressure gradient between the fluid streams, the heat exchanger material has to withstand a larger stress. This in return would increase the size of the heat exchanger which will reduce the power density, possibly changing the entire design of the AHTR.

The heat exchanger material not only has to withstand the stresses at a high temperature, but should also be chemically stable in the presence of molten salt, as molten salt tends to be corrosive (McConohy and Kruizenga 2014).

Before a heat exchanger can operate in a nuclear reactor it has to undergo several tests and licensing processes. Tests can be done by building a small scale heat exchanger, but it has to be based on a plausible design of the heat exchanger that can withstand the unique conditions it is subjected to while meeting all the requirements.

2. PROBLEM STATEMENT

The intermediate heat exchanger (IHX) required for the AHTR requires a compact novel design to successfully operate within the unique thermal, pressure and chemical conditions it is subjected to while successfully handling the heat load required for the AHTR as efficiently as possible.

3. PROJECT SCOPE

The aim of this project is to design an intermediate heat exchanger for the AHTR that will successfully transfer the heat from the core to a molten salt storage. The heat exchanger should be able to withstand the thermal, pressure and chemical conditions it is subjected to.

4. METHODOLOGY

The design method for a heat exchanger should be consistent with the life-cycle design of an engineering system and should contain the following stages.

- Problem Statement
- Concept Development
- Detailed Design
- Design Evaluation
- Operation Considerations

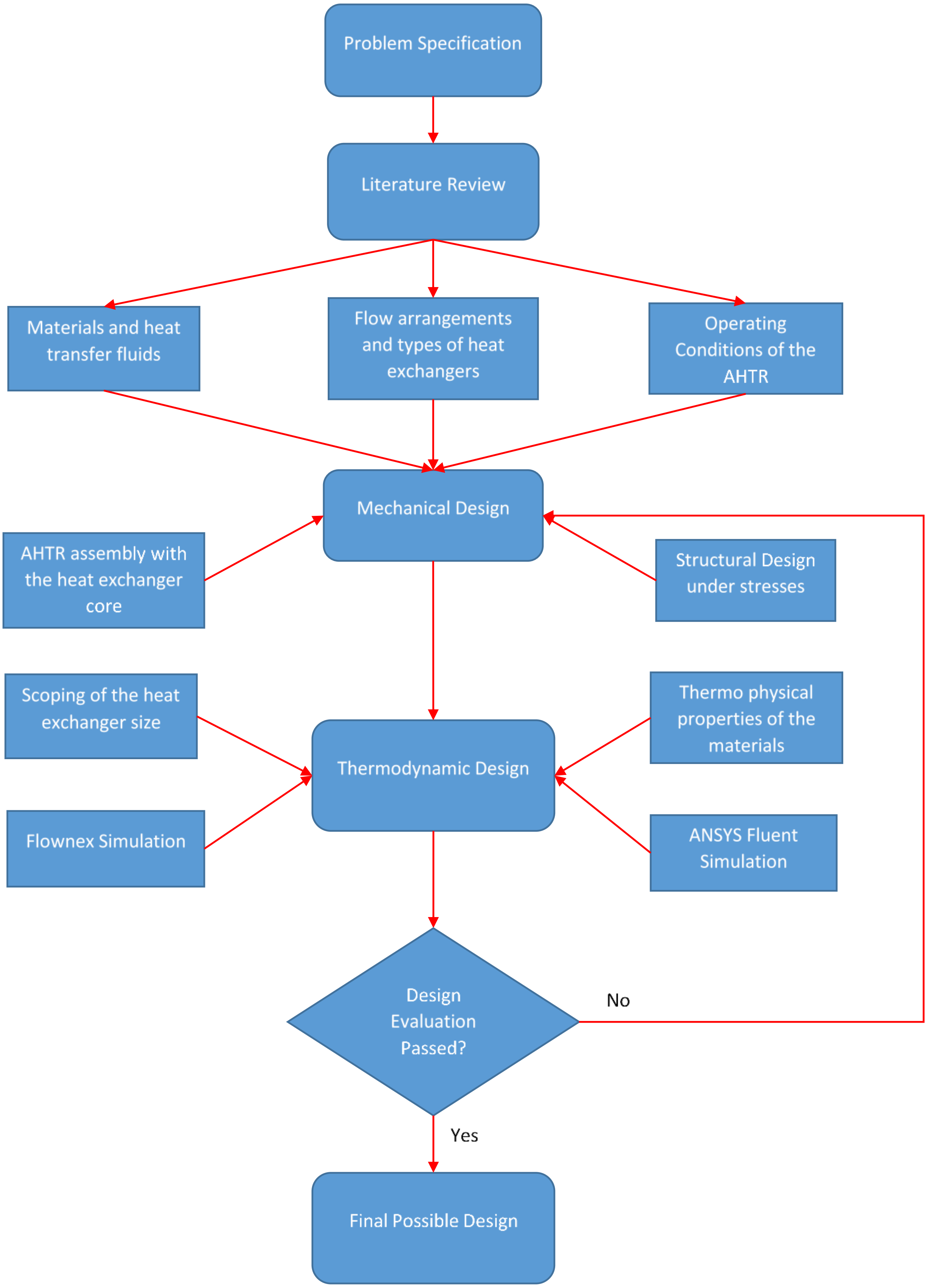
Problem Specification
Literature Review
Materials and heat transfer fluids
Flow arrangements and types of heat exchangers
Operating Conditions of the AHTR
Mechanical Design
AHTR assembly with the heat exchanger core
Structural Design under stresses
Scoping of the heat exchanger size
Thermo physical properties of the materials
Thermodynamic Design
Flownex Simulation
ANSYS Fluent Simulation
Design Evaluation Passed?
No
Yes
Final Possible Design

5. LITERATURE REVIEW

HEAT EXCHANGER DESIGN CONSIDERATIONS

The IHX is an equivalent Class1/Class2 high-temperature component and has to be designed to agree with the ASME Boiler and Pressure Vessel Code, Section III. The IHX design process will involve a balance in geometry size and acceptable pressure drops, while taking into account the thermal hydraulic properties of materials involved as well as the fabrication and fouling issues.(Sabharwall, Kim et al. 2011) The fabrication process of the IHX depends on the type of heat exchanger used and the materials involved in the heat exchange process. These processes can include casting, additive manufacturing, conventional welding or diffusion welding.(Sabharwall, Clark et al. 2014)

Here are a few key challenges when designing a heat exchanger for nuclear application:

1. Material properties at high temperatures and high pressure differentials.

2. Tritium permeation through heat exchanger material could cause contamination on secondary side.

3. Advanced heat exchanger design types lack operational experience.

4. Joining and construction processes.

5. Maintenance and inspection of heat exchangers.

HEAT EXCHANGERS TYPES

Heat exchangers are used to transfer thermal energy between two or more fluids where there is a temperature gradient. Different heat exchanger designs are used to fit the unique requirements of each system to ensure optimal heat transfer. The heat exchanger design is a complex problem that requires a deeper analysis than the heat-transfer. Production costs, weight and size play an important role in the final design.(Hesselgreaves, Law et al. 2016)

Heat exchangers are classified into several types based on different characteristics of the design. When looking at the flow configuration of the design heat exchangers are divided into four main types.

1. In a parallel-flow heat exchanger the two streams of fluid enter at the same end, follow the same flow direction and then leave at the same end.
2. In a counter-flow heat exchanger the two streams of fluid move in opposite directions.
3. In single-pass cross-flow one fluid flows at right angles to the other fluid.
4. In multi-pass cross-flow one fluid moves back and forth across the flow direction of the other fluid.

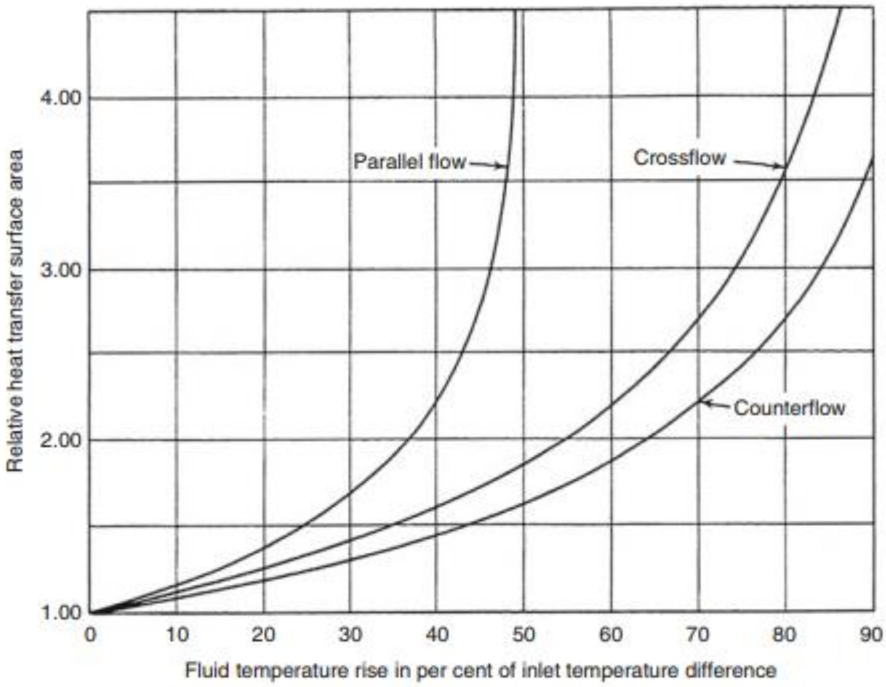

Figure 4: Relative heat transfer area required for different fluid configurations

From Figure 4 we can see that if the fluid temperature change is a small percentage of the temperature gradient then all the different types of flow configurations require roughly the same heat transfer area; the parallel-flow heat exchangers are mainly used in this region. Cross-flow and counter-flow heat exchangers require smaller heat transfer area with each design type having its own characteristics.(Hesselgreaves, Law et al. 2016)

Furthermore heat exchangers can be classified into two types when looking at the heat transfer process:

1. In an **indirect contact** heat exchanger the two streams of fluid are separated by a heat transferring medium so that the two fluids effectively never make direct contact.
2. In a **direct contact** heat exchanger the fluids are not separated by a wall and are directly in contact with each other.

Heat exchangers can also be classified by the constructions type and even though there are countless unique designs they are divided into the following groups:

TUBULAR HEAT EXCHANGERS

Tubular heat exchangers are very common and are manufactured in many sizes and flow arrangements. They can also be used in a wide spectrum of temperatures and pressures. They have a relatively low construction cost, which is the main reason for its popularity. Tubular heat exchangers can have different fluid characteristics like liquid-liquid, liquid-gas and gas-gas where both fluids are pumped through the heat exchanger. A common example of a tubular heat exchanger is a shell-and-tube heat exchanger and can be seen in Figure 5.(Kays and London 1984)

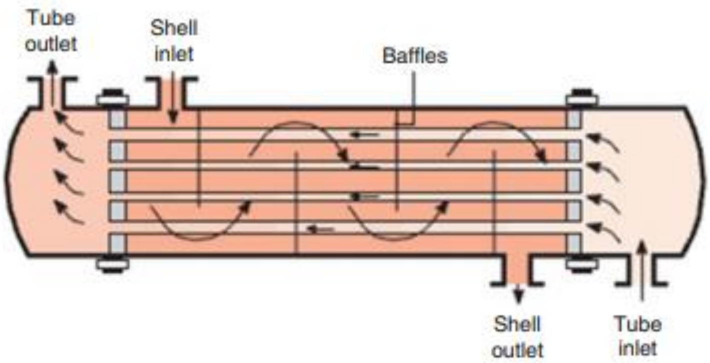

Figure 5: Shell-and-Tube Heat exchanger

PLATE HEAT EXCHANGERS

Plate heat exchangers are constructed with thin plates that separate the heat transfer fluids. These plates can be configured to be smooth or corrugated. Due to the geometry of these heat exchangers high temperatures and pressure differences in fluids are not ideal. Plate heat exchangers are mainly used in gas-gas and gas-fluid configurations as large surface contact of the plates make up for the lower heat transfer coefficients of a gas. (Kays and London 1984)

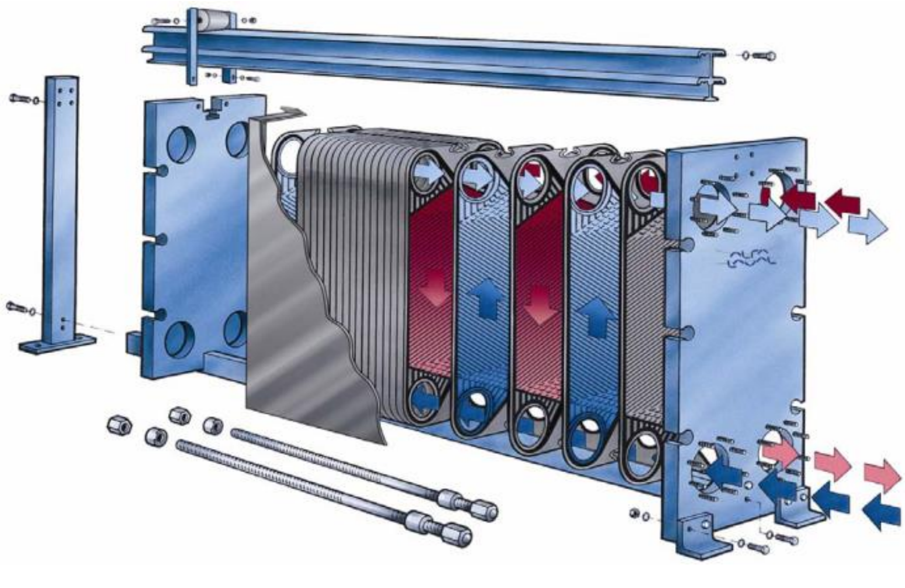

Figure 6: Plate heat Exchanger

PLATE AND FIN HEAT EXCHANGERS

In plate and fin heat exchangers the compactness factor can be increased compared to normal plate heat exchangers. In this design a flat plate is used to separate several corrugated fins and it can support cross-flow, counter-flow or parallel-flow configurations. Plate and fin heat exchangers are mainly used in gas-gas applications and are limited to an operating temperature and pressure of 800°C and 10 atm respectively.(Kays and London 1984)

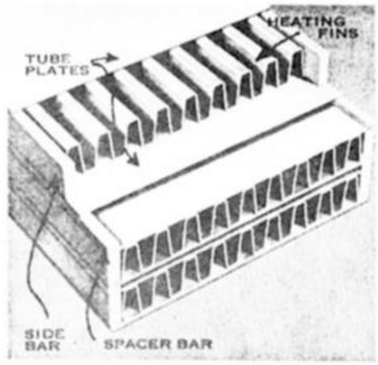

Figure 7: Plate and Fin heat Exchanger

PRINTED CIRCUIT HEAT EXCHANGER

A printed circuit heat exchanger (PCHE) has one of the highest compact factors of heat exchangers available today. A PCHE consists of many flat metal plates containing tiny grooves created by chemical milling. The metal plates are then diffusion bonded, creating a solid heat exchanger with tiny fluid passages. PCHE's are typically made from stainless steel and can handle high temperatures and pressures depending on the design and material. PCHE's can be used in gas-gas, liquid-gas and liquid-liquid fluid configurations and can be designed for any flow configuration. PCHE's are more expensive when compared to standard tubular heat exchangers. They also require very clean fluid to pass through the channels as the narrow passages are easily blocked.(Hesselgreaves, Law et al. 2016)

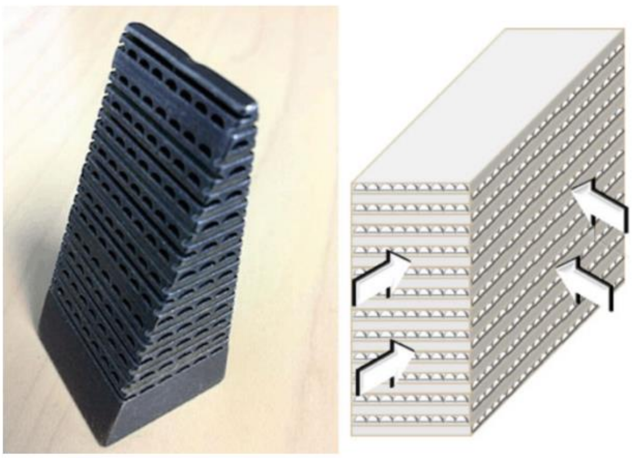

Figure 8: Printed Circuit Heat Exchanger

PCHE duct shape

The shape of the fluid duct has an impact on the stress distribution in the material. In a semi-circular duct, as in a PCHE, a stress concentration occurs at the channel tip as can be seen in Figure 10 and Figure 9.(Lee and Lee 2014)

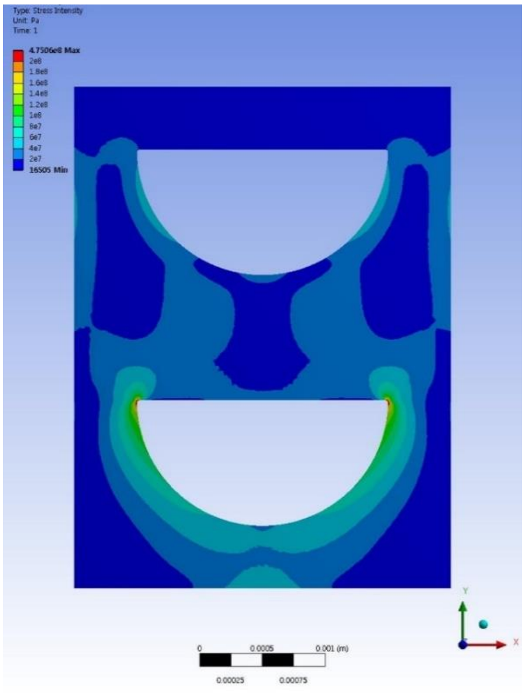

Figure 9: Stress distribution in a PCHE channel

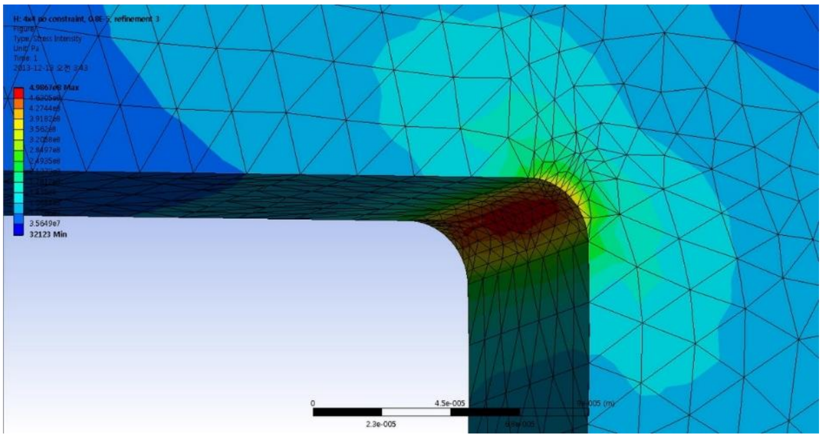

Figure 10: Stress concentration in a semi-circular duct

In a ductile material the stress concentration will ease out over time due to the edge smoothing out when creep occurs. In a brittle material like silicon carbide, the stress concentration will be present for a longer period and could cause cracks and eventually a rupture in the material.(Lee and Lee 2014).

Plate configuration

A PCHE is constructed by diffusion bonding several plates together. The small channels on the plates can be in several different configurations. In the literature most models only consider a singular flow configuration like counter-flow or parallel-flow. In reality this is not possible as the fluid streams have to be separated at the heat exchanger headers. This means that in a certain part of a counter flow heat exchanger there would be a portion that would experience cross-flow and this could influence the overall effectiveness of the heat exchanger.

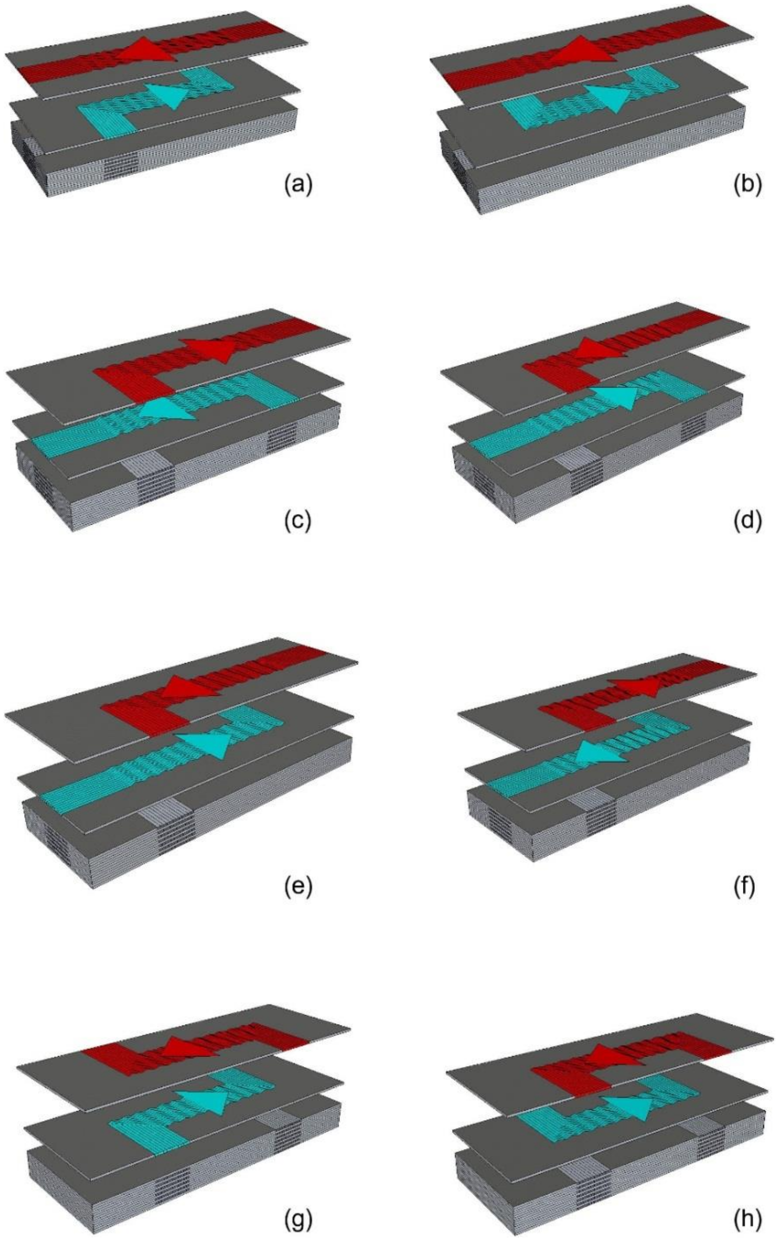

Figure 11: Plate configurations

A study done by (Son, Lee et al. 2015) determines the effect of different plate configurations on the effectiveness. In the study the plate configuration and the length of the heat exchanger is changed to see the effect it has on the effectiveness. Figure 11 illustrates all the different counter-flow heat exchangers with their header inlet configurations.(Son, Lee et al. 2015)

The width of the heat exchanger was kept constant and the length and flow configuration in the headers was changed.

Figure 12 demonstrates a plate from configuration a) and it can be seen that if the width is kept constant and the length decreases, the heat exchanger would tend to be a cross-flow heat exchanger. As the length increases it would tend to be a counter-flow heat exchanger.

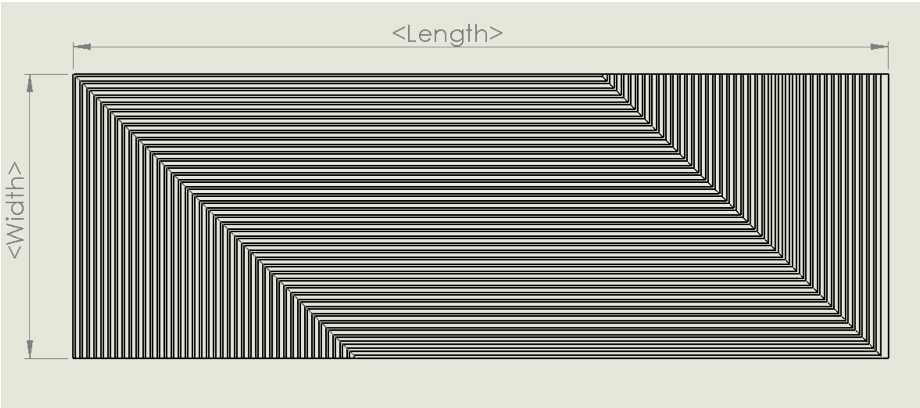

Figure 12: PCHE plate example of configuration a)

Figure 13 shows the results obtained from the study. It can be seen that as the length decreases the change in effectiveness becomes more prominent. Some of the plate configurations even show an increase in effectiveness over the sole counter-flow configuration.

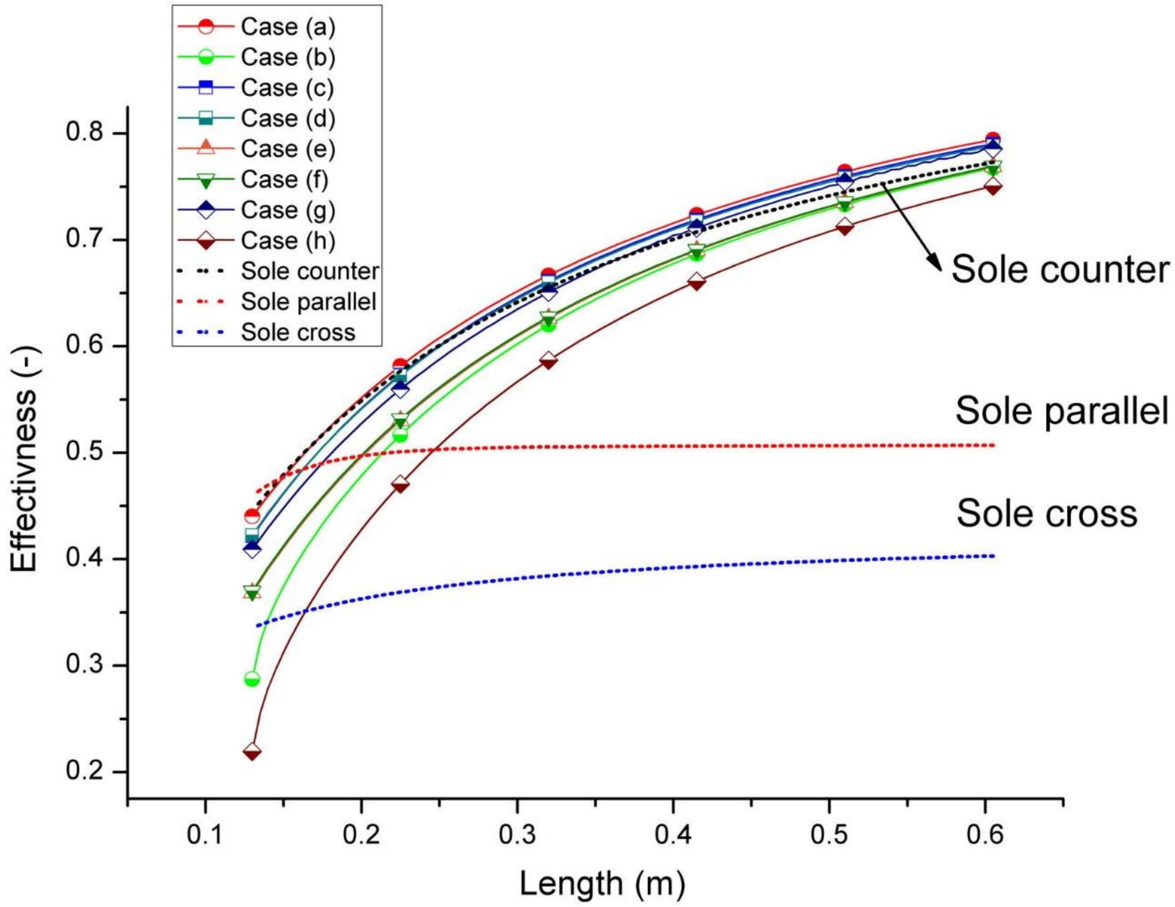

Figure 13: Plate configuration results (Son, Lee et al. 2015)

The width is kept constant in this study. This means that a length to width ratio of the heat exchanger can be calculated that only depends on the length of the heat exchanger. The effectiveness change can then be plotted against the length to width ratio. I can apply this ratio to my design to ensure that my effectiveness will not be influenced too much by the plate configuration and to justify that a counter-flow simulation will be accurate in reality.

HEAT EXCHANGERS FOR AHTR APPLICATION

From the heat exchangers studied a suitable option should be chosen that would be ideal for the AHTR. The analysis is summarized in the table below.

Heat Exchanger Type	AHTR Compatibility	Comment
Tubular heat exchangers	Average	There is a wide range of different tubular heat exchangers and they can be designed to fit the temperatures and pressures that the AHTR reactor's heat exchanger requires. They are cheap, but tend to be big compared to other options.
Plate heat exchanger	Weak	The pressure differential of 9MPa is not ideal for a Plate heat exchanger configuration.
Plate and Fin heat exchangers	Good	Plate and Fin heat exchangers can handle relatively large pressures and is a good option for the AHTR's heat exchanger.
Printed Circuit heat exchangers	Very Good	The Printed circuit heat exchanger is a very good option for an AHTR heat exchanger. It has a very high compact factor and can handle high pressures.

MATERIALS

The Material selection for the high temperature heat exchanger is made by considering the operating conditions as well as considering the fluids that will be passing through the heat exchanger. The candidate materials should exhibit high-temperature tensile and creep strength and a resistance to corrosion when exposed to the molten salt and high temperature helium. Any material that is used commercially should meet the standard requirements that are given by the ASME codes.

The material for the IHX structure has to satisfy all the requirements specified by the operating conditions. Certain key properties are looked at to determine whether the material will be suitable and they are:

Tensile Strength – The material should be able to withstand the stresses caused by operating and accident conditions.

Corrosion – Given the maximum temperature and pressure, the material should show corrosion resistance toward operating fluids at these conditions to ensure a maximum operating lifetime.

Creep – The material creep under the operating conditions should be a minimum for the lifetime of the reactor.

The alloys that show the best corrosion resistance to molten salt are not codified for nuclear applications. The alloys that are suitable for nuclear use are more corrosive and will result in a shorter lifetime of the heat exchanger. There is a great need for experimental data so that more materials can be added to the nuclear application code.

MOLTEN SALT

The molten salt storage is based on the technology development of concentrated solar power. These power plants store the heat generated by the solar panels in the molten salt where it can be used to generate steam at a later stage. Currently these plants use a nitrate molten salt that stores heat at temperatures up to 550°C. The next generation of solar power plants aim to increase the storage temperatures to a range of 600°C-800°C in order to improve the efficiency of the power plant. These higher temperatures exceed the stability temperature of the nitrate salt and chloride salts are promising candidates to replace them. These chloride salts are more corrosive than the nitrate salts and the material selection of containment should be taken into account.(Liu, Wei et al. 2017)

The use of solar salts as heat transfer fluid is well documented in operating Concentrating Solar Power plants.(Kearney, Kelly et al. 2004) The salts mostly used in the industry are shown in

Table 4.

Salt	Composition
Solar Salt	60 wt% $NaNO_3$, 40 wt%KNO_3
HITEC®	40 wt% $NaNO_2$, 53 wt%KNO_3, 7 wt% $NaNO_3$
HITEC® XL	48 wt% $Ca(NaNO_3)_2$, 45 wt%KNO_3, 7 wt% $NaNO_3$

Table 4: Different Molten Salts

(Khare, Dell'Amico et al. 2012)

<u>Solar Salt Properties</u>

The AHTR's thermodynamic cycles are designed with a molten salt loop containing Solar Salt. In order to correctly simulate the heat exchanger the thermo physical properties of Solar Salt is required.

Figure 14 shows experimental data done on several molten salts. From the data it is seen that the specific heat of Solar Salt stays relatively constant in the operating temperature range. The assumption can be made that the specific heat of Solar Salt is constant at 1.62 J/g*K throughout the heat exchanger. (Zhang, Cheng et al. 2018)

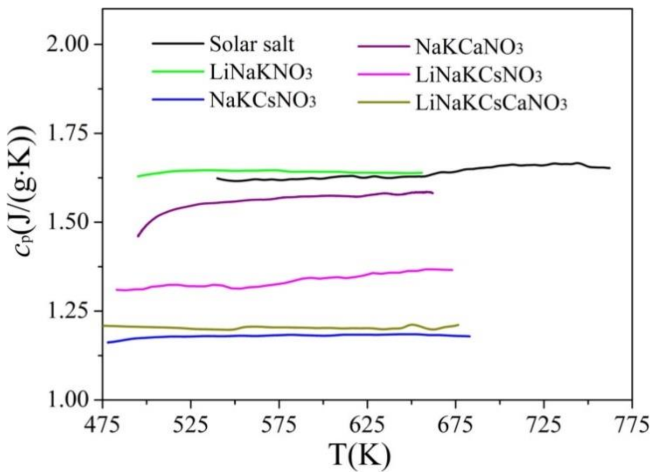

Figure 14: Solar Salt Specific Heat

The densities of several molten salts can be seen in Figure 15. From the experimental data it can be seen that the density follows a straight line with negative gradient as the temperature increases. The density of the solar salt can be calculated by using the following equation:

$$\rho = 2.346 - 0.0007650 * T$$

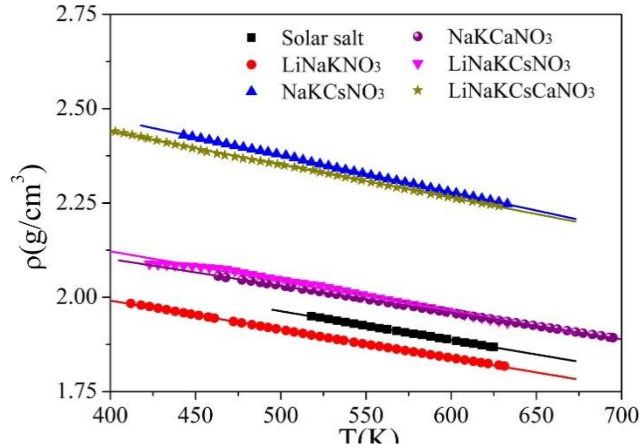

Figure 15: Solar salt Density

The viscosity of several molten salts can be seen in Figure 16. Viscosity of solar salt can be calculated as a function of temperature with the following equation:

$$\mu = 0.1286 * e^{\left(\frac{15.23}{R*T}\right)}$$

Where R is the universal gas law constant.(Zhang, Cheng et al. 2018)

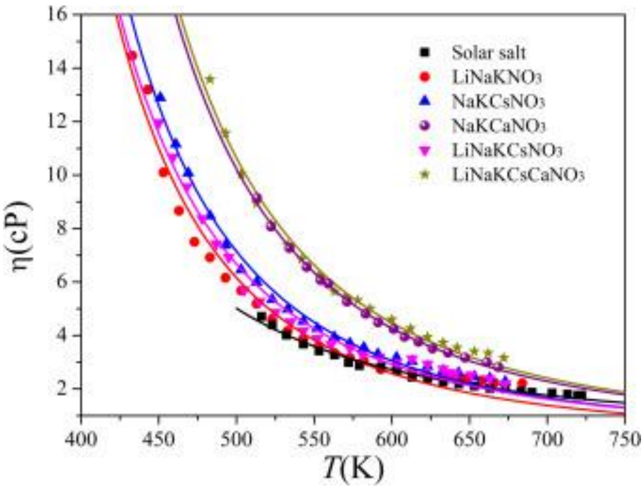

Figure 16: Solar Salt Viscosity

HIGH TEMPERATURE NICKEL-BASED ALLOYS

High temperature nickel based alloys are the logical choice for strength and corrosion resistance as the elevated temperatures increases corrosion kinetics. These alloys are more expensive than Fe-based alloys and the lifetime cost needs to be considered when a material is selected.(Kruizenga and Gill 2014)

Incoloy 625

Incoloy 625 shows excellent corrosion resistance against solar salt at a temperature of 600°C with a metal loss of 16.8 µm/year extrapolated based on 3000 h data. The corrosion resistance at 680°C increases to 594 µm/year.(McConohy and Kruizenga 2014)

Incoloy 800H

Incoloy 800H is an iron-nickel-chromium alloy that shows moderate strength and good oxidation resistance at high temperatures. The H grade controls the carbon, aluminium and titanium contents in combination with a high temperature anneal to deliver an alloy with improved resistance to creep. In the ASME III, division 1, subsection NH Incoloy 800H is only qualified up to a temperature of 427°C to be used in nuclear systems. Test performed by the German HTR program however provides allowable stresses for their design up to a temperature of 1000°C.(Mitchell and Smit 2006)

Inconel 617

Inconel 617 is a nickel based alloy designed for structural use at high temperatures and pressures. A draft ASME code has provided allowable stress values for the PBMR IHX for a 100 000 hour design period at temperatures of 980°C.(Mitchell and Smit 2006). Alloy 617 is not currently allowed in the ASME Code section III (nuclear use) and can be found in Section VIII, Division 1 (for non-nuclear applications). More data on creep-fatigue in different loading scenarios are needed to improve the predictive capability on the creep fatigue. System pressure testing is also required to examine corrosion especially with changes in Helium purity.(Natesan, Moisseytsev et al. 2009)

Hayness Alloy 230

Alloy 230 is a nickel based alloy designed for structural use at high temperatures and pressures. Similarly, to Alloy 617, Alloy 230 is included in the ASME Code for non-nuclear applications but yet to be approved for nuclear applications(Natesan, Moisseytsev et al. 2009). Hayness Alloy 230 shows excellent corrosion resistance against solar salt at a temperature of 600°C with a metal loss of 23.6 µm/year extrapolated based on 3000 h data. The corrosion at 680°C increases drastically to 688 µm/year. (McConohy and Kruizenga 2014)

Hastelloy N

Hastelloy N is a nickel based alloy that was developed at Oak Ridge National Laboratories as a fluoride molten salt containment material. It shows excellent corrosion resistance, good tensile strength and good machinability. At 649°C it showed no weight gain when exposed to an oxidation material after 170 hours. The low corrosion that Hastelloy N experiences makes it a viable option for a compact heat exchanger design due to the large effect even a small amount of corrosion will have on the small fluid channels. Hastelloy N can be diffusion bonded.(Sabharwall, Clark et al. 2014)

FE-BASED ALLOYS

Fe-based alloys form a passive oxide layer on the contact surface consisting of Fe_3O_4 when exposed to molten nitrate salts. The formation of the oxide layer makes nitrate salts less corrosive when compared to other molten salts. Nitrate salt reaches thermal instability at elevated temperatures and is generally operated at around 500°C. This makes the use of common alloys a good option as lower corrosion rates are observed at these temperatures.(Patel, Pavlík et al. 2017)

Stainless Steel AISI 304

AISI 304 shows no corrosion products when exposed to solar salt and HITECH® XL at a temperature of 390°C for 2000 hours. At 550°C AISI 304 achieved minimal corrosion that would be satisfactory for operation for the lifetime of a CSP plant.(Fernandez, Lasanta et al. 2012)

Stainless steel AISI 403

AISI 403 show no corrosion products when exposed to solar salt and HITECH® XL at a temperature of 390°C for 2000 hours, however suffered severe corrosion at a exposed temperature of 550°C.

SILICON CARBIDE (SIC)

Silicon Carbide has high gas tightness, high thermal conductivity, low specific weight and a high corrosion resistance making it an ideal option for a heat exchanger material. Depending on structure and ceramic bonding, SiC ceramics can be classed as porous SiC materials, such as silicate bonded, recrystallized or nitride bonded SiC, or dense SiC materials, like reaction bonded infiltrated or sintered SiC.(Fend, Völker et al. 2011)

The most common design for a SiC heat exchanger is the plate and fin heat exchanger. The construction process starts by forming the green compact plates into the desired shape with the ceramic slurry. These plates can then be treated with a coating substance to improve corrosion resistance. After the plates have been formed they are sintered together at temperatures between 1800°C and 2000°C. To join the plates together ceramic slurry is added to the connection surfaces and the plates are once again sintered together. These joint plates have strength of 75%-90% of the bulk SiC. After the sintering of all the plates are completed, the final assembly can be constructed.(Schulte-Fischedick, Dreißigacker et al. 2007)

There are however several joining methods of SiC that include diffusion bonding using various active fillers, transient eutectic phase methods such as Nano-Infiltration and Transient Eutectic-phase (NITE), laser joining, selected area chemical vapour deposition, glass–ceramic joining, solid state displacement reactions and pre-ceramic polymer routes.(Katoh, Snead et al. 2014)

A study done on the oxidation of SiC in a solar salt environment showed that when exposed to solar salt at temperatures of up to 600°C, a thin layer of SiO_2 would form on the surface, protecting the SiC against further oxidation.(Cheng, Ye et al. 2018)

SiC has a very low tritium and deuterium permeation rate and is used in some applications as a protective layer to prevent the permeation of tritium and deuterium.(Wright, Durrett et al. 2015)

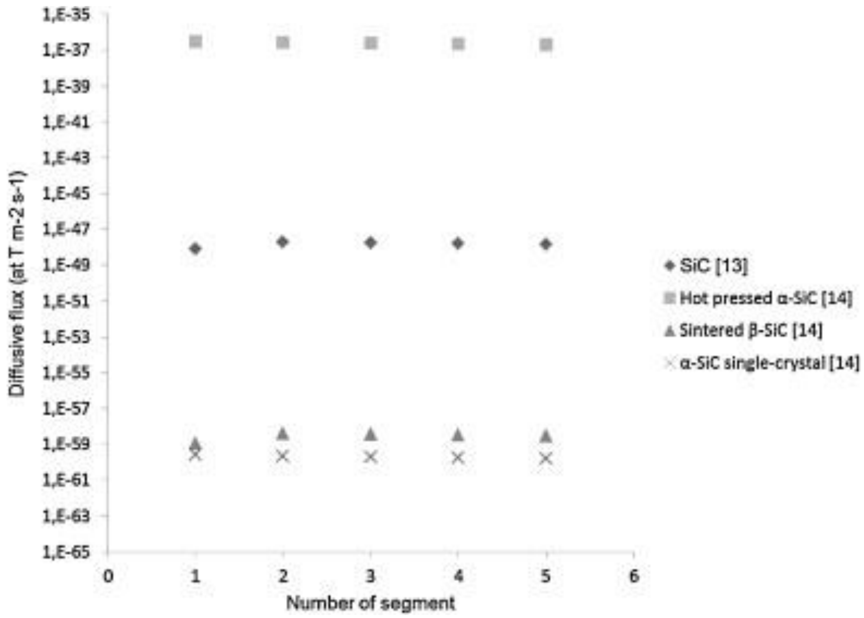

Figure 17: Tritium permeation through SiC

Figure 17 shows results of tritium permeation through several SiC samples in a PCHE with CO_2-Lead configuration. This demonstrates SiC as a good tritium permeation barrier.(Fernández and Sedano 2013)

Table 5: Materials summary

Material	**Tested Temperature**	**Corrosion exposed to Solar Salt (mm/year)**	**ASME Code for Nuclear Application**	**ASME Design Stress (MPa)**	**Sources**
Incoloy 625	600°C	0.0168	Not Permitted	178	(McConohy and Kruizenga 2014)
Incoloy 800H	600°C	0.01-0.03	Permitted to Temperature of 427°C	75.7	(Carling and Bradshaw 1986)
Inconel 617	600°C	Testing Required for Solar Salt	Not Permitted	143	(Natesan, Moisseytsev et al. 2009)
Hayness Alloy 230	600°C	0.0236	Not Permitted	153	(McConohy and Kruizenga 2014)
Hastelloy N	649°C	0	Not Permitted	40.7	(Sabharwall, Clark et al. 2014)
SS AISI 304	558 °C	0.21	Permitted to Temperature of 427°C	93.3	(Sohal, Ebner et al. 2010)
Silicon Carbide	600°C	SiO_2 layer of 0.2 mm forms to prevent further corrosion	Not Permitted	36.46	(Cheng, Ye et al. 2018)

LITERATURE REVIEW SUMMARY

Eskom AHTR design specifications

The design specifications for the IHX were derived from existing thermodynamic cycles and schematic drawings available for the Eskom AHTR. From the thermodynamic cycle design the boundary conditions of the IHX are known and a heat exchanger effectiveness can be calculated. The schematic drawings of the AHTR give a good indication of the volume allocation and heat exchanger assembly.

Heat exchanger type

Several heat exchanger types were looked at in the literature. Heat exchanger types like shell-and-tube, plate-and-fin and printed circuit heat exchangers show potential application in the AHTR. A PCHE design is chosen due to its high compactness and ability to handle high pressure differences in the fluids. The flow configuration of the heat exchanger is to be determined in the design and will be chosen to minimize the heat exchanger's size.

Material Selection

The temperature that the IHX would reach in normal operating conditions is higher than any of the possible materials allowable operating temperature for nuclear use according to the ASME code. This shows the need for data considering materials for high temperature nuclear reactors. For a turbine failure condition where helium at 1200°C and 9MPa reaches the IHX, none of the metals will be in the allowable design stress. Silicon carbide seems like a good candidate material that can withstand the accident temperatures; however the brittleness of silicon carbide gives it a high fracture failure probability under high pressures especially when a heat exchanger design like a PCHE with a high number of pressure channels is used. If silicon carbide is used as a heat exchanger under high pressures, multiple tests are required to create an ASME code draft in order for it to be licensed for nuclear use.

An extra safety system should be designed that would passively cool the helium in case of an accident condition so that the extreme conditions never reach the IHX. For this study the assumption is made that such a safety system exists and therefore the material that will be used in the IHX is chosen based on a combination of strength and corrosion resistance at normal operating conditions.

For this design Hastelloy N is chosen as the IHX material due to the high corrosive resistance and acceptable mechanical properties. Hastelloy N can also be diffusion bonded and is suitable with a PCHE design.

6. THE DESIGN PROCESS

STAGE 1: MECHANICAL DESIGN

The mechanical design for the IHX should be able to withstand the pressure and temperature stresses throughout the lifetime of the reactor. The design should make sense in the AHTR assembly and should be as small as possible.

In order to minimize the heat exchanger size, the walls between the fluids should be minimized. The thickness of the solid walls will be limited by the pressure difference in the two fluids so that the internal stress of the material caused by the fluids does not exceed the allowable stress at the operating temperature.

To prevent mechanical failure the dimensions for channel pitch and plate thickness should be larger than the minimal design criteria. The stress in the heat exchanger can be written as a function of pressure difference in the fluids, wall thickness and wall density.(Hesselgreaves, Law et al. 2016)

$$\sigma_D = \Delta p(\frac{1}{N_f t_f} - 1)$$

Where

Δp = the pressure difference in the two fluids

σ_D = the stress in the material

N_f= the wall density

t_f= the wall thickness

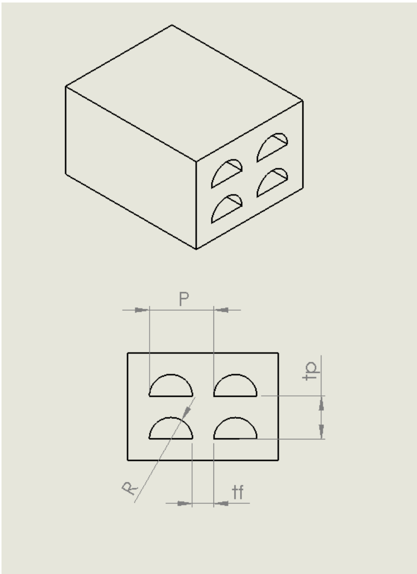

Figure 18: PCHE channel configuration

From this equation a maximum allowable stress can be substituted into σ_D and a minimum wall thickness can be calculated along with a specified wall density. N_f can be calculated as

$$N_f = 1/P$$

Where P is the Pitch of the channels illustrated in Figure 18.

To calculate the minimum plate thickness it can be assumed that the pressurized channel is a thick walled cylinder with an inner radius R and an outer radius of tp. The thickness can then be calculated as function of allowable stress and applicable pressures.

$$t_p \geq R\sqrt{\frac{\sigma_{max} + P_{primary}}{\sigma_{max} + 2P_{secondary-}P_{primary}}}$$

Where

t_p= Plate thickness

R = channel radius

σ_{max} = maximum allowable stress

$P_{primary}$= Pressure of Helium

$P_{secondary}$=Pressure of Solar Salt

The IHX should be in a shape that fits the AHTR design assembly. The current AHTR design allocates a circular shape for the heat exchangers and forms part of the power generating unit as seen in Figure 19. (Fox 2017)

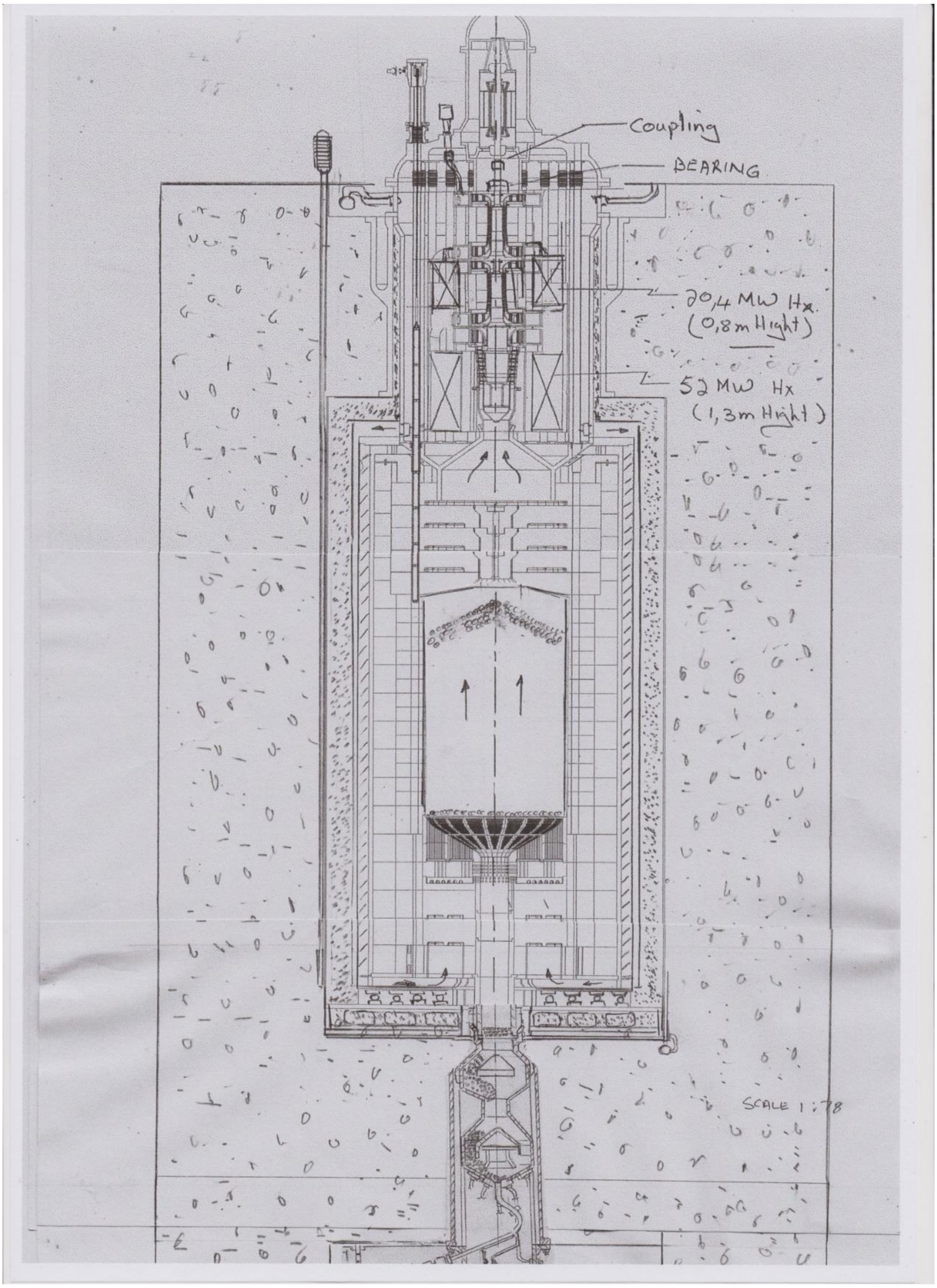

Figure 19: AHTR reactor scaled drawing with heat exchanger allocation

Figure 19 shows a scaled drawing of the AHTR reactor with heat exchangers allocated in the power generating unit. This design was based on an AHTR reactor where the IHX was a helium to supercritical CO2 component, therefore it is suspected that the size for a helium to molten salt IHX would be different. Even though the secondary cycle fluid has changed the space allocated to the heat exchangers in Figure 19 will be used as a starting design point. The total volume that the heat exchangers use was calculated to be around 6.3 m^3 with an average radius of 0.95 m as seen in

Figure **20**.

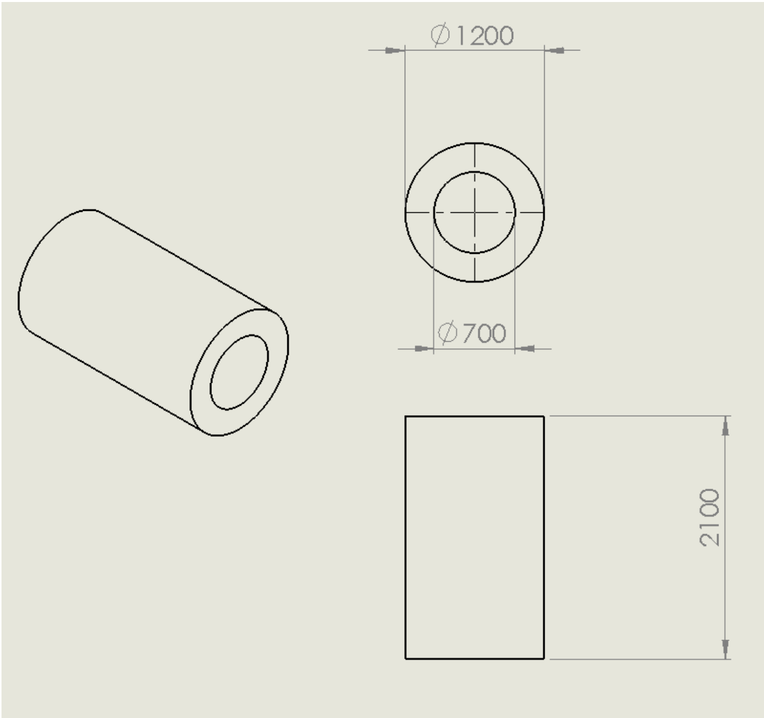

Figure 20: Heat exchanger estimated Volume

The helium to molten salt cycle design contains a high temperature IHX with a pre-cooler and two intercoolers. All the heat exchangers should fit into the allocated volume. The assumption is made that there is a correlation between the heat exchanger's size and the heat duty it performs. We can therefore estimate a volume allocation per heat exchanger by looking at its heat duty.

Table 6: heat exchanger volume allocation

Heat exchanger name	Heat Duty (kW)	% Total Heat Duty	Volume allocation (m^3)
High temperature IHX	14908	18.75	1.18
Pre-Cooler	21550	27.10	1.71
Intercooler LP	21550	27.10	1.71
Intercooler HP	21496	27.05	1.7

STAGE 2: SCOPING SIZE

1. The first step is to calculate the heat exchanger effectiveness ε with the following equation:

$$\varepsilon = \frac{\dot{Q}}{Q\dot{m}ax} = \frac{C_h(T_{h,i} - T_{h,o})}{C_{min}(T_{h,i} - T_{c,i})} = \frac{C\,(T_{c,o} - T_{c,i})}{C_{min}(T_{h,i} - T_{c,i})}$$

Where C_h and C_c are the hot and cold stream heat capacity rates, one of them being C_{min} unless the heat exchanger is balanced and both are equal.

2. Next the flow configuration should be chosen for the IHX. In this case a counter-flow configuration is chosen because of the higher compact factor that can be achieved with it as space in the AHTR design is limited.

3. Now that the flow configuration is chosen the number of transfer units (Ntu) can be determined by using a ε-Ntu equation found in (Hesselgreaves, Law et al. 2016).

4. From the Ntu value the N value for each stream can be calculated with the following formula.

$$\frac{1}{Ntu} = \frac{1}{N_h(C_h/C_{min})} + \frac{1}{N_c(C_c/C_{min})}$$

The Ntu is known where N_h and N_c are calculated by estimating one of them. In general for a liquid to gas configuration N = 1.1Ntu for the gas side.

5. Using the values of N, allowable pressure drop and mean properties, the mass velocity (G) can be calculated. From the value of G the flow area (A_c) can be calculated

$$G = \frac{\dot{m}}{A_c}.$$

6. From surface choices and hydraulic diameter the Reynolds number for a channel can be calculated. This is influenced by heat exchanger type. The data for several heat exchangers demonstrated in (Hesselgreaves, Law et al. 2016) was used and the printed circuit heat exchanger was chosen as a suitable option for the IHX.

7. The following equation can then be used to calculate the length L for each fluid path.

$$L = \frac{d_{h^2}}{\eta}(\frac{\dot{m}PrN}{4Nu})$$

The symbol η is the viscosity, Pr the Prandtl number and Nu the Nusselt number calculated with mean temperatures and pressures. The hydraulic diameter and mass flow illustrated by d_h and $\dot{m}$ respectfully.

The equations mentioned above can be used to scope the design for the heat exchanger and is used in EES as seen in Appendix A. If the effectiveness, pressure drop and flow diameters are specified the fluid path lengths for each fluid can be calculated. The results for the scoping design give a good indication of the ratios between size and flow areas.

Table 7 shows an example of results obtained from the scoping program. It is assumed that both flow channel diameters are equal. Note that the fluid path lengths are not equal. In the case of a parallel or counter flow heat exchanger an average fluid path length can be used as a scope.

Property	Solar Salt Channel	Helium Channel
Heat Duty	14915 kW	14915 kW
Inlet Temperature	480.629 °C	630°C
Outlet Temperature	517.303°C	510.766°C
Heat Capacity	1.62 kJ/kg.K	5.192 kJ/kg.K
Mass Flow	244.765 kg/s	24.092 kg/s
Inlet Pressure	Atmospheric	2369.154 kPa
Maximum Pressure Drop	(not the critical channel)	23.45 kPa
Effectiveness	0.7982	0.7982
Flow Area	0.2388 m^2	0.2262 m^2
Length of fluid path	1.83 m	0.1 m
Diameter	0.002 m	0.002 m

Table 7: Initial Scoping design

Figure 21 shows what the relationship between the flow channel diameter and the fluid path length should be in order to achieve the desired effectiveness and pressure drop.

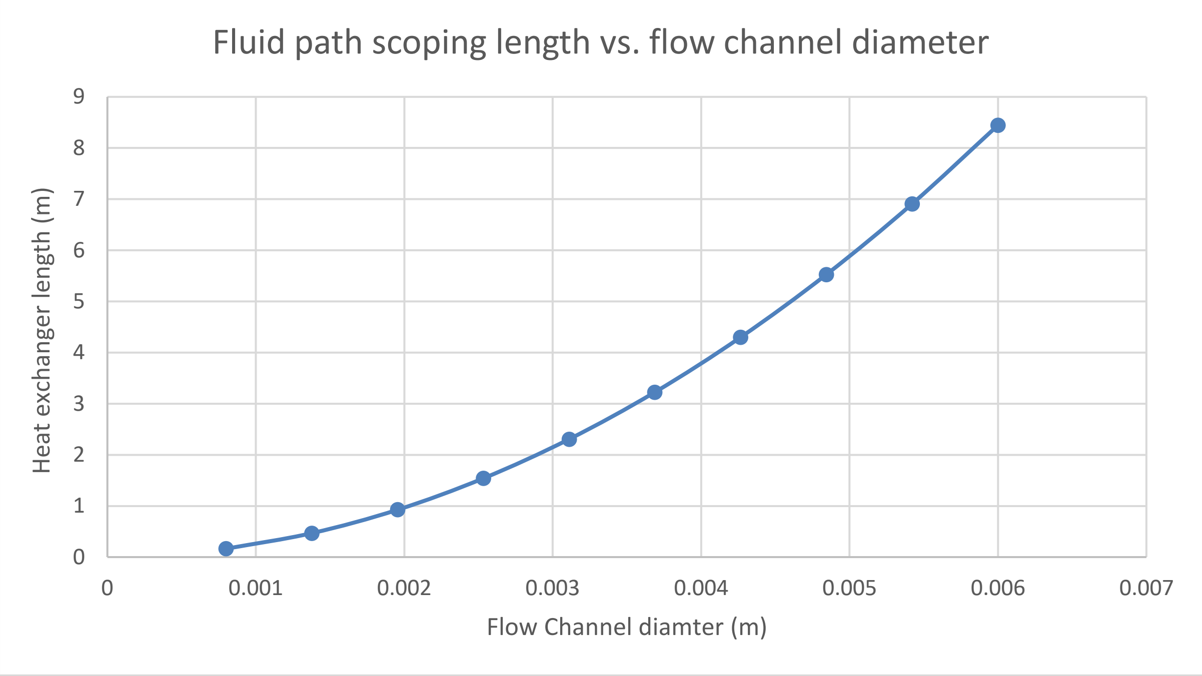

Figure 21: Scoping Stage, Fluid path length vs. flow channel diameter

It should be kept in mind that the smallest possible heat exchanger should be used, and that a larger channel diameter and fluid path length would result in a larger heat exchanger. The graphical results obtained from Figure 21 shows an increase in fluid path length as the channel diameter increases. Pressure drop is directly proportional to the fluid path length and inversely proportional to the channel diameter, therefore the results make sense as a pressure drop was specified. Now that the scoping phase is complete the rating phase can commence.

STAGE 3: RATING PHASE

The rating phase is done by using the recuperator element in Flownex. The recuperator element can be calculated in a parallel and counter flow configuration and is modelled in a discretised fashion rather than a lumped system. Flownex has the ability to do a Monte Carlo sensitivity analysis on several variables.

<u>Assumptions</u>

- The amount of fluid channels for each fluid is equal. This allows the simulation to only randomize one flow area as the other flow area would be proportional to the diameter ratio of the two channels.
- Hastelloy N is used as the recuperator material.
- Surface roughness of 30 µm is used for the fluid channels.

- Inputs like the total heat transfer area, wall thickness and pitch are functions of the channel diameters and are calculated in an excel add-on within Flownex with formulas described in the mechanical design section.

- Laminar Nusselt number for a PCHE is used.(Hesselgreaves, Law et al. 2016)

Figure 22: Flownex Model Visuals

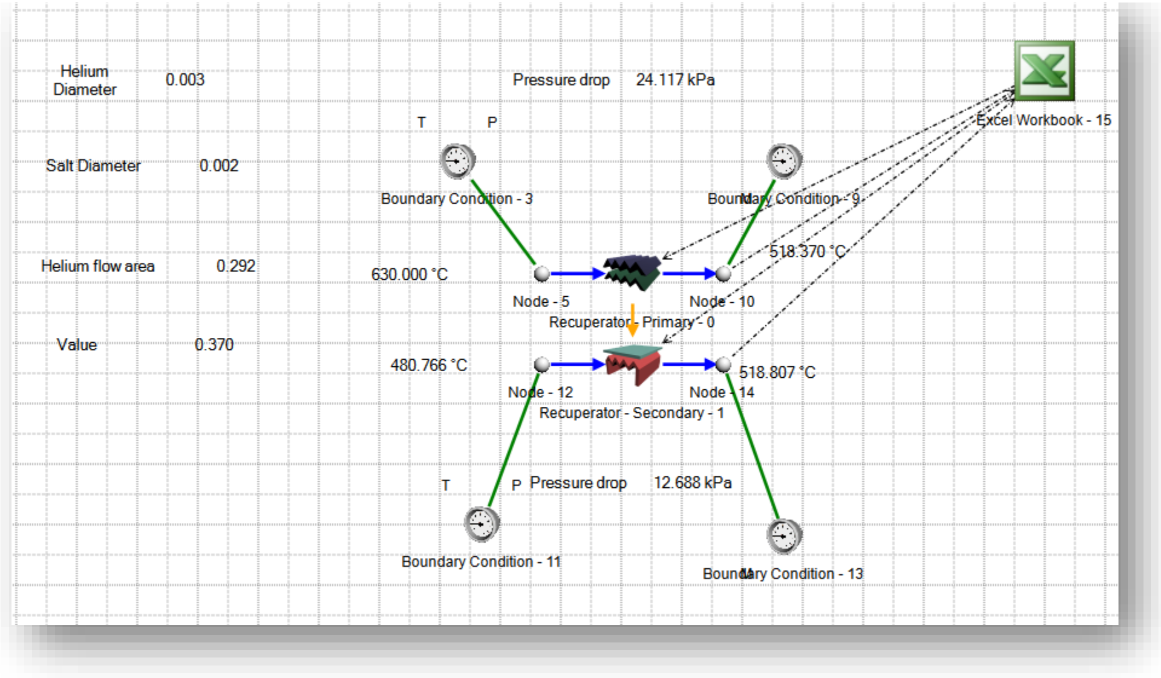

FLOWNEX EQUATIONS

The validity of the Recuperator model is subject to the following constraints:

- The Mach number is smaller than one over the entire length of the flow channel for both sides.

- The flow channel cross-sectional area is completely filled with fluid over the entire length of the flow channel for both sides.

The validity of the Recuperator model is subject to the following assumptions:

- Constant specific heat of the fluid throughout an increment. This assumes a small temperature difference across an increment. This assumption is valid only for small increments.

- Ideal gas behaviour in case of compressible fluids.

- The convection heat transfer coefficients are constant throughout an increment of the discretised heat exchanger.

- Axial conduction within the separation plate material is neglected in the calculation of heat transfer rates.

- The heat transfer in the fluid through diffusion through the fluid itself is disregarded.

- In the case of transient flow events, the friction factor for the flow in the tube is obtained from an equation based on the Moody diagram, which was developed for steady-state flow conditions.

- The stagnation temperature (and stagnation pressure in case of compressible flows) is related to static temperature (and static pressure in case of compressible flows) using equations applicable to ideal gasses with constant specific heat.

Consider the incremental recuperator shown in Figure 23. The subscripts *p* and *s* refers to the primary side and the secondary side respectively. The figure shows an incremental counter flow heat exchanger which could be represented as a thermal resistance network, shown on the right hand side of the figure.

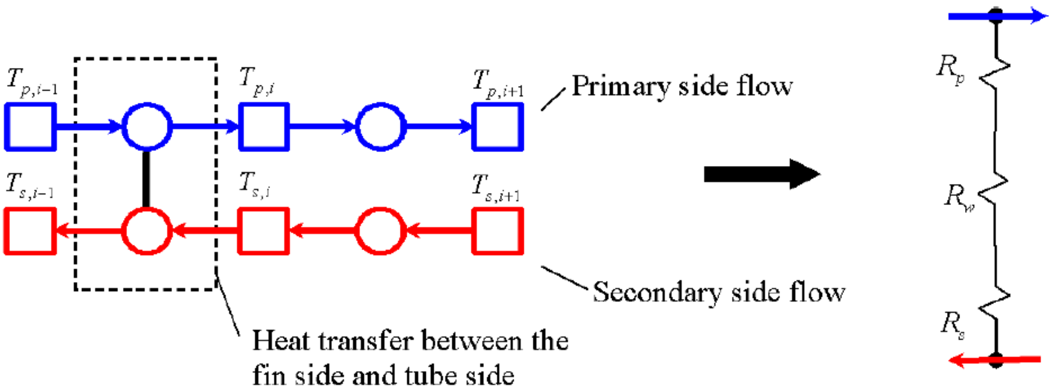

Figure 23: Elemental Recuperator

The heat transfer link between the primary side and secondary side flow comprises of convection links with solid nodes as shown in Figure 23. Each flow node has a convection link to an associated solid node which forms an incremental heat exchanger.

The maximum heat transfer in this incremental heat exchanger,

$$\dot{Q}_{max} = C_{min}\left(T_{s,i} - T_{p,i-1}\right)$$

Where

C_{min} =minimum value of the heat capacity rates [J/K.s] defined as:

$$C_{min} = \min\left(\left(\dot{m}c_p\right)_p, \left(\dot{m}c_p\right)_s\right)$$

For steady-state heat transfer, the heat transfer rate to or from the primary side fluid stream Q_p is calculated by:

$$\dot{Q}_p = \dot{m}_p c_{p,p}\left(T_{p,i-1} - T_{p,i}\right)$$

Where

$T_{p,\,i-1}$ = inlet temperature of the primary side increment fluid stream [K],

$T_{p,\,i}$ = outlet temperature of the primary side increment fluid stream [K].

And similarly, the steady-state heat transfer rate to or from the secondary side fluid stream, Q_s, is calculated by:

$$\dot{Q}_s = \dot{m}_s c_{p,s}\left(T_{s,i} - T_{s,i-1}\right)$$

Where

$T_{s,\,i}$ = inlet temperature of the secondary side increment fluid stream [K],

$T_{s,\,i-1}$ = outlet temperature of the secondary side increment fluid stream [K].

The effectiveness of the heat exchanger, Ɛ, is calculated with:

$$\varepsilon = \frac{\dot{Q}_p}{\dot{Q}_{\max}}$$

The heat transfer, Q_p, from the primary side flow stream to the solid node is given as:

$$\dot{Q}_p = U_p A_p \left(\frac{T_{p,i-1} + T_{p,i}}{2} - T_w \right)$$

Where

$T_{p,\,i-1}$ = the upstream primary side node static temperature [K],

$T_{p,\,i}$ = the downstream primary side node static temperature [K],

T_w = the solid node static temperature [K],

A_p = the total primary side heat transfer area for the specific increment [m2] and

U_p = the overall heat transfer coefficient for the primary side of the heat exchanger [J/kg.K].

Similarly, the heat transfer, Q_s, from the solid node to the secondary side flow stream is given as:

$$\dot{Q}_s = U_s A_p \left(T_w - \frac{T_{s,i} + T_{s,i-1}}{2} \right)$$

The overall heat transfer coefficient for the primary side is given by:

$$U_p = \left[\frac{1}{\eta_{fp} \lambda_p} + \frac{A_p}{A_m} \frac{t_w}{2k} \right]^{-1}$$

Where

η_{fp} = primary side heat transfer efficiency (Example: Fin efficiency) [-]

λ_p = primary side heat transfer coefficient [W/m2.K]

A_p = total primary side heat transfer area for the specific increment [m2]

A_m= average area of the separating material between the two fluid streams, assumed to be A_s [m2]

t_w = metal the wall thickness of the separating material between the primary and secondary flow streams [m]

k = separating material thermal conductivity [W/m.K]

Similarly, the overall heat transfer coefficient for the secondary side is given by:

$$U_s = \left[\frac{A_p}{A_s} \frac{1}{\eta_{fs} \lambda_s} + \frac{A_p}{A_m} \frac{t_w}{2k} \right]^{-1}$$

The surface heat transfer coefficients, λ_p and λ_s, can be calculated by either using the Nusselt number calculated by the Dittus Boelter correlation or by using the Colburn *j* relation. If the surface heat transfer coefficients are calculated with the Dittus-Boelter equation, the laminar Nusselt number is specified by the user and the following equation is used for the turbulent region:

$$\frac{\lambda D_h}{k} = a_3 \left(0.023\, Re^{0.8} Pr^{n} \right)$$

Where

k = thermal conductivity of the tube side fluid,

n = 0.4 for heating and 0.3 for cooling of the fluid in the tube and

a_3 = a multiplier value which accounts for non-circular geometries, which is 1 in the case of a circular geometry.

Boundary Conditions

Table 8: Flownex Boundary Conditions

Property	Value
Helium Inlet Temperature	630°C
Solar Salt Inlet Temperature	480.629 °C
Helium Inlet Pressure	2369.154 kPa
Solar Salt Inlet Pressure	100 kPa
Helium Mass Flow	24.092 kg/s
Solar Salt Mass Flow	244.765 kg/s

Monte Carlo Sensitivity Analysis Setup

The sensitivity analysis was set to deliver 5000 iterations.

Table 9: Monte Carlo Inputs

Property	Low Value	High Value	Distribution Type
Helium Diameter	0.001 m	0.005 m	Uniform
Salt Diameter	0.001 m	0.005 m	Uniform
Helium Flow Area	0.05 m^2	0.5 m^2	Uniform
Fluid Path Length	0.1 m	1.5 m	Uniform

Parallel flow configuration

The sensitivity analysis produced 5000 different heat exchangers that are in parallel flow configuration. The results where filtered out to only show heat exchangers that have a pressure drop below 20 kPa.

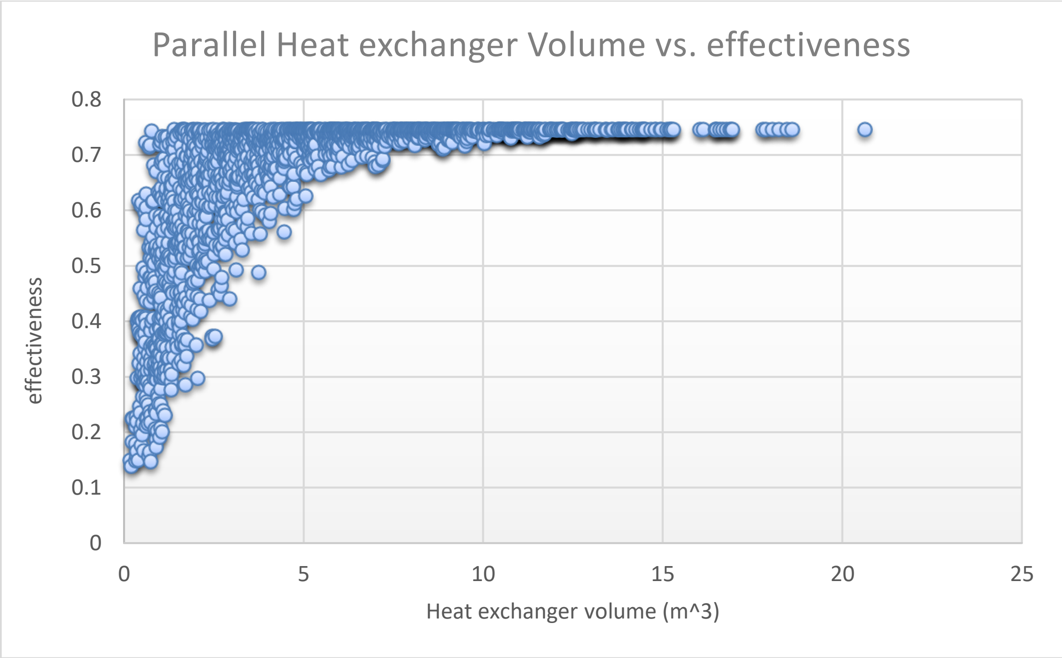

Figure 24: Parallel Heat exchanger Volume vs. effectiveness

From the Flownex results it can be seen that the effectiveness of the parallel flow heat exchanger never reaches the desired effectiveness of 0.79. A high temperature difference at the inlet causes high heat transfer, gradually decreasing as the two streams reach an equilibrium temperature. The desired effectiveness can be reached in a parallel configuration but that would mean changing the flow area ratio drastically, resulting in a larger heat exchanger.

From the results we can conclude that a parallel flow heat exchanger would not be suitable for the IHX

<u>Counter flow configuration</u>

The sensitivity analysis produced 5000 different heat exchangers that are in counter flow configuration. The results where filtered out to only show heat exchangers that have a pressure drop below 20 kPa.

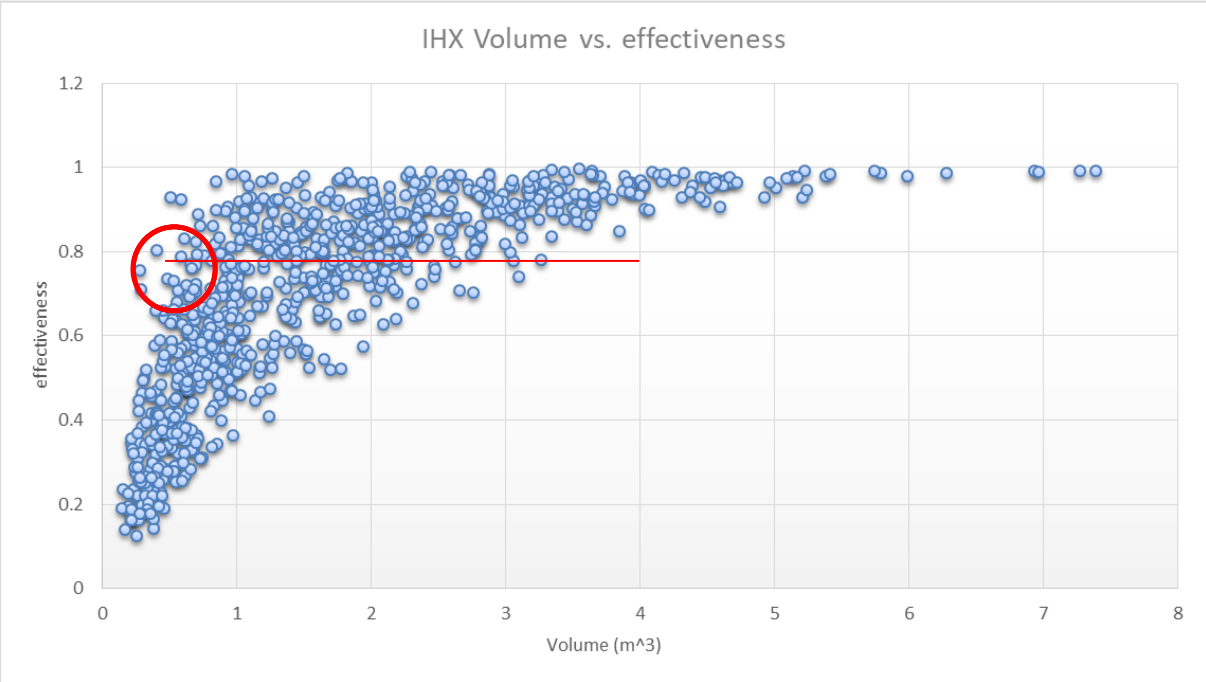

Figure 25: Counter flow Heat exchanger volume vs. effectiveness

In Figure 25 the heat exchanger effectiveness plotted against the volume of the heat exchanger is shown. It can be seen that the heat exchanger volume is directly proportional to the effectiveness. This makes sense as the larger the heat exchanger becomes, the larger the heat transfer area becomes and therefore a higher effectiveness. All of the heat exchangers seen in the plot on the 0.8 effectiveness line would be suitable for the outlet conditions required by the design, however most of these heat exchangers are very large. The smallest possible heat exchanger that could deliver an effectiveness of 0.8 should be chosen.

Size is not the only variable to look at when practically implementing a heat exchanger. Ideally the face area of the heat exchanger should be as small as possible. The smaller the face area, the easier it is for the fluids to be distributed to the heat exchanger from the turbine. A heat exchanger with a large face area relative to its length would be impractical even though its volume is small.

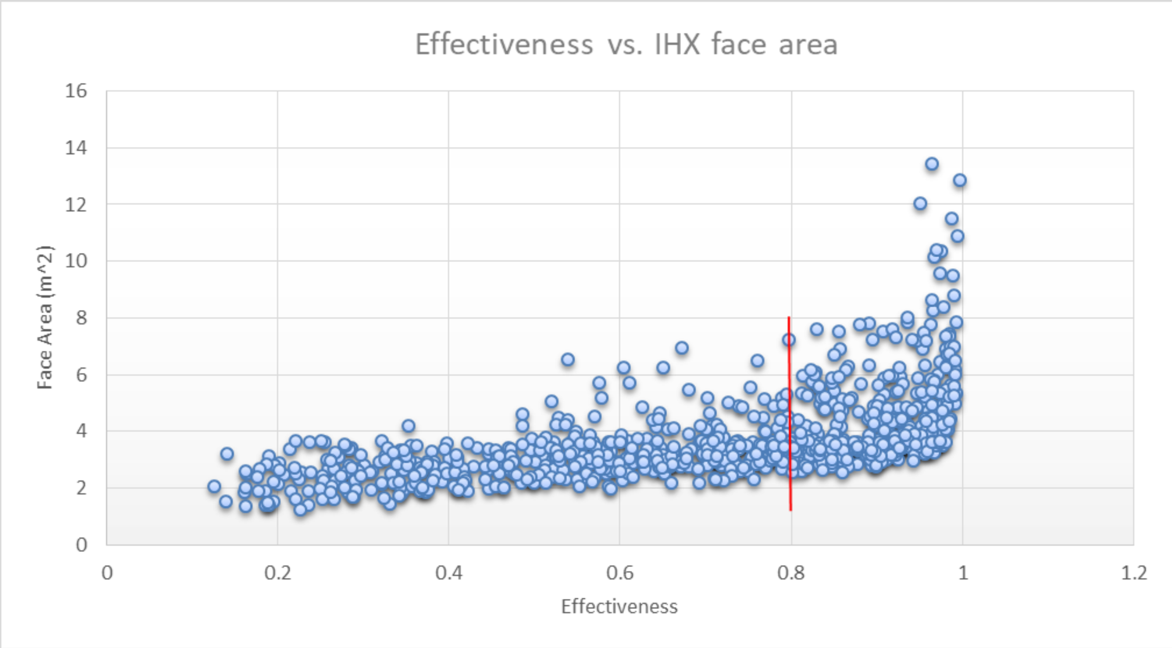

Figure 26: Effectiveness vs. Heat exchanger face area

In Figure 26 it can be seen that the face area for heat exchangers with effectiveness of 0.8 range between 4 and 10 square meters. By comparing the volume and face areas, 5 heat exchangers are chosen as possible solutions for the AHTR application and are listed in the table below.

<u>Heat exchangers selection process</u>

1. The data is sorted to only show pressure drops in the heat exchangers with a maximum of 20 kPa

2. The Reynolds number is sorted to only show heat exchangers in the laminar region. This is done to ensure that the results obtained are reliable. A Reynolds number between 2300 and 5000 will be in the transition region between laminar and turbulent flow and can have unpredictable heat transfer characteristics.

3. Data is sorted so that the face area is ranged from smallest to largest.

4. The effectiveness is filtered to show values ranging between 0.7 and 0.9

5. Heat exchangers with a small face area and acceptably small volume is chosen. For the heat exchanger volume the reference value as discussed in the mechanical design section is used.

Table 10: Selected Heat exchangers

	1	2	3	4	5
Helium channel Diameter (m)	0.00189	0.00173	0.00203	0.00165	0.00196
Solar Salt Diameter (m)	0.00198	0.00135	0.00214	0.00219	0.00233
Helium Flow Area (m^2)	0.316	0.362	0.351	0.286	0.335
Solar Salt Flow Area (m^2)	0.349	0.221	0.391	0.505	0.473
Fluid Path Length (m)	0.219	0.221	0.308	0.173	0.260
Helium Pressure Drop (kPa)	13.087	13.586	14.057	14.930	13.341
Solar Salt Pressure Drop (kPa)	4.087	14.004	4.389	1.827	2.596
Volume (m^3)	0.536	0.590	0.840	0.483	0.761
effectiveness	0.731	0.789	0.819	0.736	0.790
Face Area (m^2)	2.437	2.584	2.726	2.798	2.932

The final design is chosen by evaluating the advantages and disadvantages of each attribute.

Independent Variables

Channel Diameters

All the above heat exchangers have similar flow diameters. The flow diameter is inversely proportional to the pressure drop. The reason smaller flow diameters weren't suited for the heat exchanger is due to the large pressure drop that occurs within the smaller channels.

Flow Areas

The flow areas are also in a similar range, agreeing with the results obtained in the scoping phase. Changes in flow areas would cause velocity changes and that has a major impact on the Reynolds number. The Reynolds number is used in the heat transfer and pressure drop calculations.

Fluid Path Length

The fluid path lengths for the heat exchangers range from 0.173-0.308 m. The length should be kept in mind during the assembly of the heat exchanger. The length is directly proportional to the pressure drop in the fluid.

Dependent Variables

Helium Pressure Drop

The pressure drop in the helium is a very important variable as it is directly linked to the efficiency of the primary Brayton cycle. Heat exchanger 1 has the lowest pressure drop with heat exchanger 4 having the highest. All the pressure drops are however within the allowable design pressure drop.

Solar Salt Pressure Drop

The pressure drop in the solar salt gives a good indication of the pump that would be required to pump the salt from the storage system at the specified mass flow. The larger the pressure drop, the more energy the pump is going to need. This will have an effect on the overall efficiency of the plant. Heat exchanger 2 has the highest pressure drop in the solar salt with heat exchanger 4 having the lowest.

Volume

The volume is one of the most important dependant variables. The volume is directly linked to the cost of the heat exchanger due to material cost and the manufacturing processes. Heat exchanger 4 has the lowest volume with heat exchanger 3 having the highest.

Effectiveness

The effectiveness of the heat exchanger is the most important criteria that has to be met. It can be seen that the heat exchangers chosen don't have an effectiveness of exactly 0.798. This means that small changes in the independent variables should still be made to achieve the desired effectiveness. These small changes would however affect the size and pressure drops once again. The closest heat exchanger to the desired effectiveness is heat exchanger 5 with an effectiveness of 0.790.

Face Area

The face area of the heat exchanger should be as small as possible. A small face area is desired to simplify the fluid transport to the heat exchanger core. If the face area is too large, more additional losses could come into play through the connecting pipes.

STAGE 4: OPTIMIZATION PHASE

In order to choose and optimize a solution for the IHX the five candidate heat exchangers mentioned in the rating phase have to be changed to deliver the desired effectiveness. Small changes to the fluid path length where changed in Flownex by using the built in designer function to ensure an effectiveness of 0.798. The five candidate heat exchangers where then compared once again.

Table 11: Optimized heat exchangers

	1	**2**	**3**	**4**	**5**
Helium channel Diameter (m)	0.00189	0.00173	0.00203	0.00165	0.00196
Solar Salt Diameter (m)	0.00198	0.00135	0.00214	0.00219	0.00233
Helium Flow Area (m^2)	0.316	0.362	0.351	0.286	0.335
Solar Salt Flow Area (m^2)	0.349	0.221	0.391	0.505	0.473
Fluid Path Length (m)	0.276	0.236	0.286	0.214	0.267

Helium Pressure Drop (kPa)	16.218	14.917	13.086	18.170	13.729
Solar Salt Pressure Drop (kPa)	5.203	15.518	4.099	2.265	2.661
Volume (m^3)	0.673	0.609	0.778	0.597	0.782
effectiveness	0.798	0.798	0.798	0.798	0.798
Face Area (m^2)	2.437	2.584	2.726	2.798	2.932

ANSYS Fluent Simulation

Symmetry heat transfer element simulation

In order to verify that the results obtained from Flownex, the five selected heat exchangers are simulated using ANSYS Fluent. It is impractical to simulate the entire heat exchanger in ANYS as it would take too much computing power. In order to simplify the model, a reoccurring geometry with correct boundary conditions can be used.

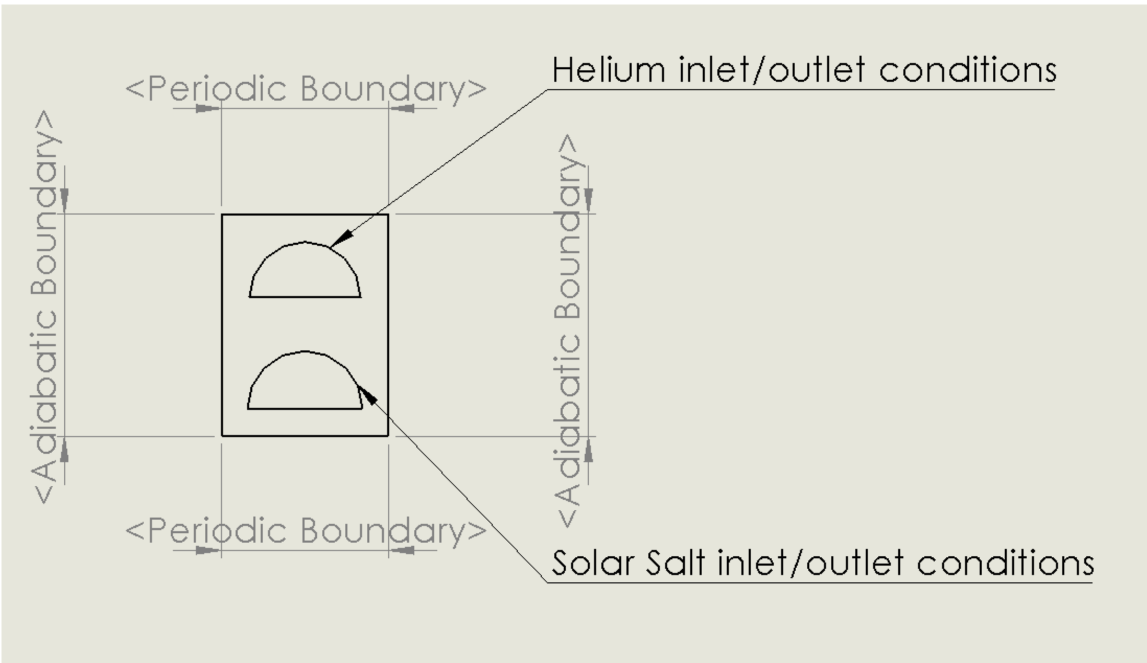

Figure 27: ANYS element boundary condition setup

ANSYS Fluent Assumptions

- The upper and lower walls of the heat transfer element have a periodic boundary condition. This is due to the repeating nature of the heat transfer element.
- Inlet temperatures and pressures for the fluids are the same as the Flownex conditions.
- The wall roughness is 30 µm.
- Hastelloy N is used as the solid material
- The walls on the side are adiabatic as heat transfer only takes place between the two different fluid streams.
- The inlet mass flows for each channel is calculated by taking the total mass flow and dividing it by the amount of channels there are in the heat exchanger. The amount of channels was calculated in the Flownex simulation and is a function of the total flow area and channel flow areas.
- The fluid flow model is selected is based on the Reynolds number calculated in Flownex.

ANSYS Fluent Simulation Method

1. The heat transfer element is drawn in Solidworks and saved as a .step file to be opened in ANSYS.
2. ANSYS is opened and a new Fluent project is started.
3. The geometry file created in Solidworks is imported.
4. The important geometry is edited so that a volume is assigned to the voids occupied by fluids.
5. A mesh is generated in the geometry.
6. ANSYS Fluent is started. All the necessary models are specified and the boundary conditions are allocated to the geometry.
7. If no solution is obtained then step 5 and 6 is repeated. A good mesh is essential to achieve a converged solution.
8. Results are analysed and compared with the help of a built in post processing component.

Meshing

Heat transfer coefficient calculations in laminar flow, using the finite volume method can be quite grid dependant due to the interaction between flow field resolution and temperature field resolution. It is therefore important that the meshing on the element is not too rigid to ensure an accurate solution.

ANSYS student v.19 was used to do the CFD simulations and unfortunately the student version is limited to a certain sized mesh. The mesh was generated to be as fine as possible within the allowable finite elements that ANSYS student allowed.

7. DESIGN RESULTS EVALUATION

HEAT EXCHANGER 1

Table 12 shows the detailed design parameters for heat exchanger 1 as calculated in Flownex.

Table 12: Heat exchanger 1 detailed Flownex parameters

Parameter	Value
Diameter Helium	0.00189 m
Diameter Solar Salt	0.00198 m
Flow Area Helium	0.316 m^2
Flow Area Solar Salt	0.347 m^2
Fluid Path Length	0.276 m
Plate thickness	0.0019 m
Heat transfer Area	369.169 m^2
Volume	0.673m^3
Face Area	2.437 m^2
effectiveness	0.798
Number of Symmetry heat transfer elements	225180
Compact factor	548.762 m^{-1}
Pitch	0.0029 m
Helium Average Reynolds Number	2176.32
Solar Salt Average Reynolds Number	426.983

Figure 28 shows the cross section symmetry element design with units being in millimetre.

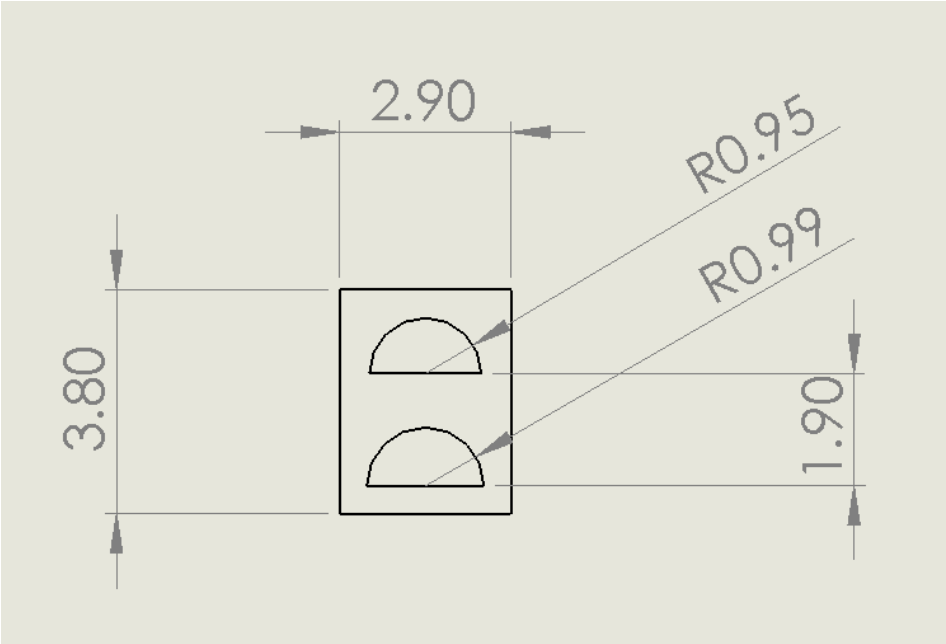

Figure 28: Heat exchanger 1 element

ANYS Fluent Results and discussion

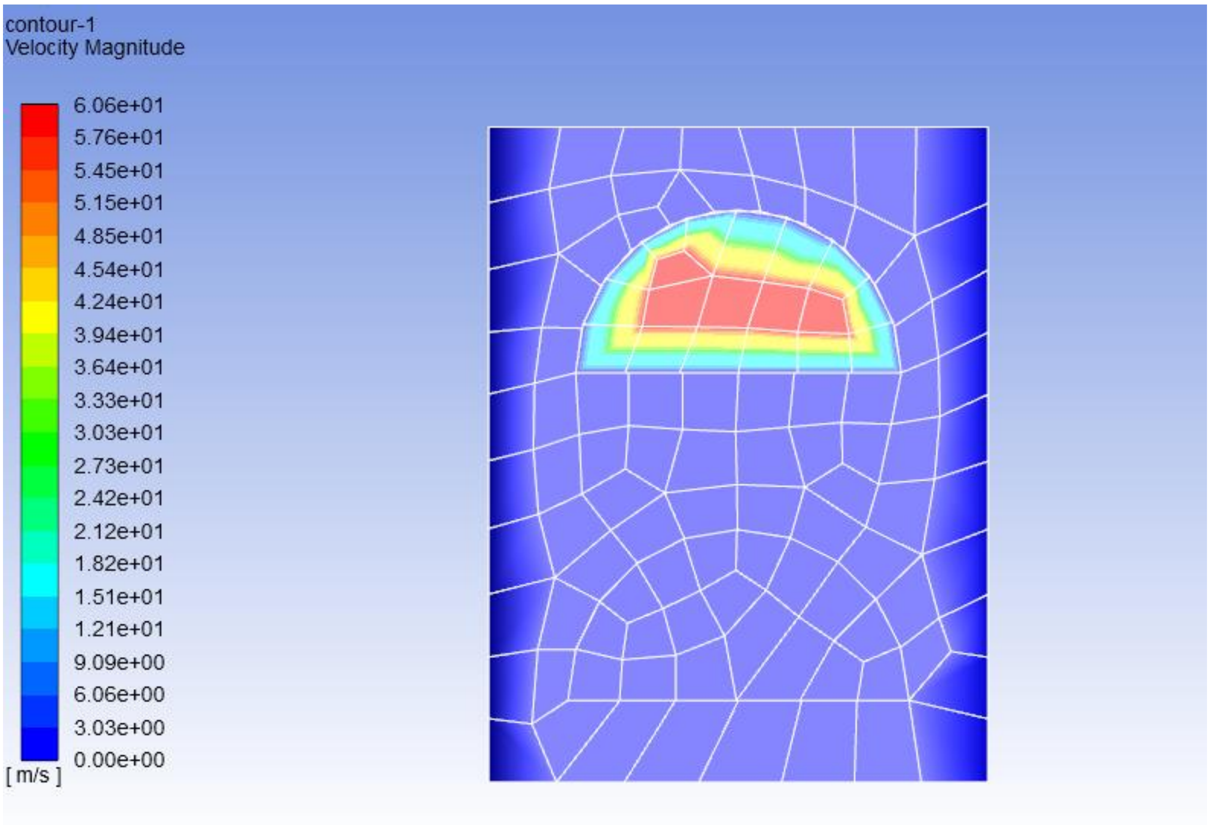

Figure 29: Heat exchanger 1 velocity magnitude

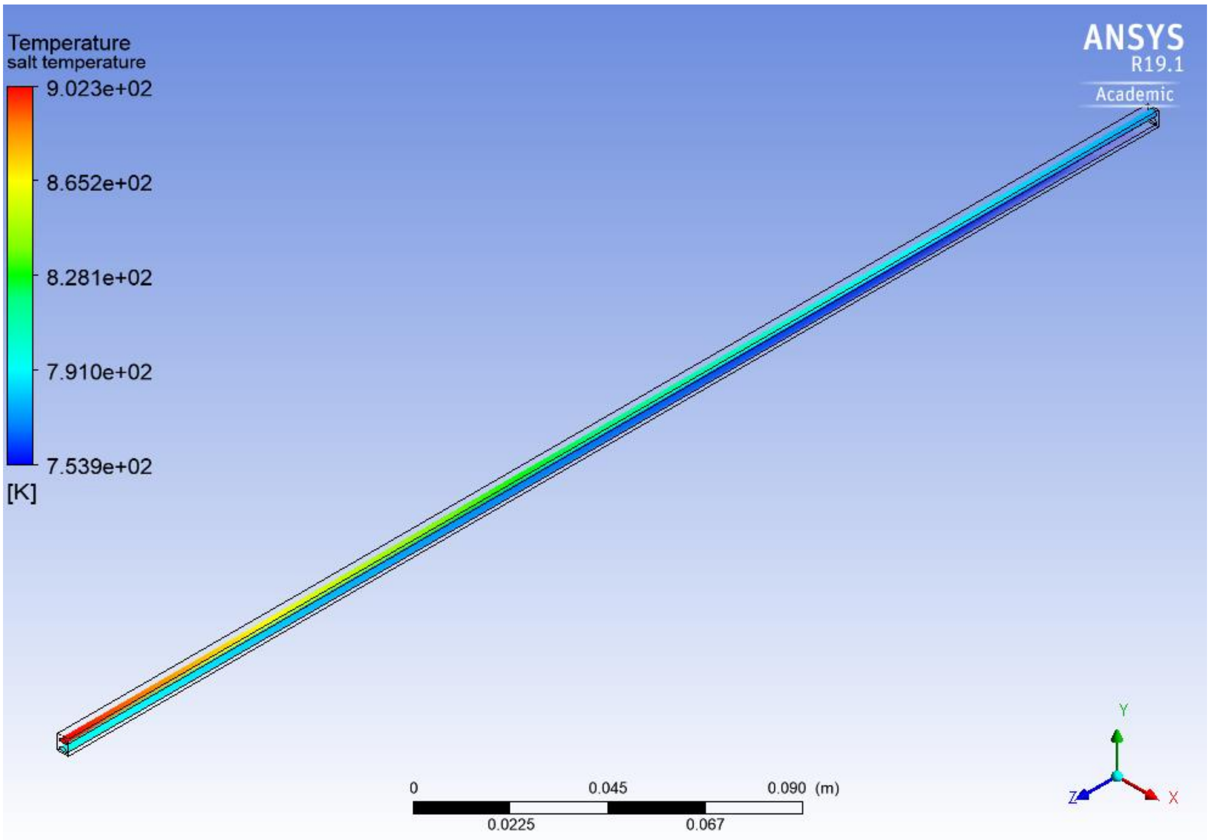

Figure 30: Heat exchanger 1 3D temperature profile

Figure 29 shows the velocity magnitude of the helium in a plane perpendicular to the flow direction. In the image we can see a slower velocity towards the wall of the helium channel which is expected.

Figure 30 shows the temperature distribution in the fluid domains. From the distribution it is clear that the flow configuration in the model is correct as the hot inlets to the fluids are on opposite sides. No irregularities in the temperature results can be seen and the distribution in temperature is smooth. Figure 30 also shows the length of the heat exchanger element relative to its flow area.

Figure 31 plots the temperatures of the fluid streams in the middle of the element component, the red values being the helium and the blue values being the solar salt. The temperature in the fluid channel will not have a constant temperature as the fluid nearer to the wall boundary will be slightly higher and therefore it can be seen that at a specific heat exchanger length there are multiple temperature values. These values still follow a typical counter-flow heat exchanger profile, indicating that the simulation setup is correct.

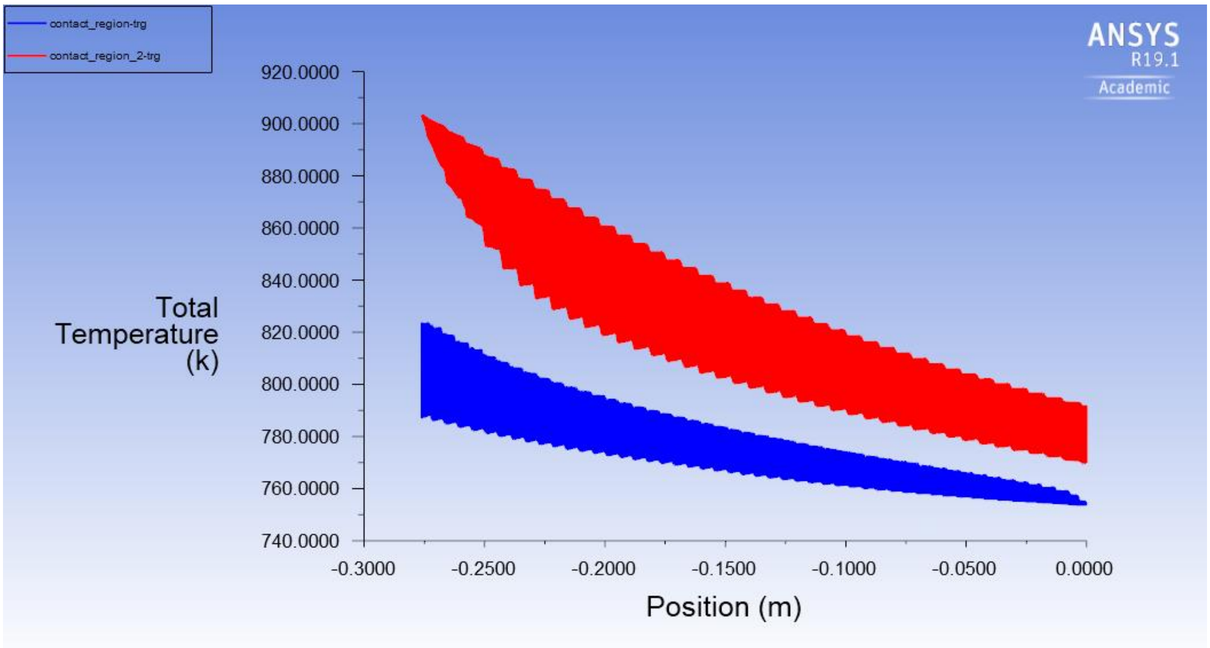

Figure 31: Heat exchanger 1 fluid temperature along the path length

In order to compare the results obtained in ANYS to Flownex, a built in area average calculator is used in the post processing component. The area average calculator is applied to the inlet and outlet areas of the geometry so that the average inlet and outlet conditions can be compared.

Table 13: Heat exchanger 1 results comparison

Parameter	ANSYS Fluent	Flownex	Absolute Difference
Helium Inlet Temperature (°C)	630	630	0
Solar Salt Inlet Temperature (°C)	480.766	480.766	0
Helium Outlet Temperature (°C)	509.763	510.919	1.156

Solar Salt Outlet Temperature (°C)	522.186	518.334	3.852
Helium Pressure Drop (kPa)	13.28	16.218	2.938
Solar Salt Pressure Drop (kPa)	4.212	5.203	0.991
Effectiveness	0.806	0.798	0.008
Helium Inlet Density (kg/m^3)	1.26	1.26	0
Helium Outlet Density (kg/m^3)	1.44	1.44	0
Helium Inlet Velocity (m/s)	60.597	60.597	0
Helium Outlet Velocity (m/s)	53.06	53	0.06
Solar Salt Velocity (m/s)	0.39	0.39	0

In the results comparison table the outlet temperatures of the ANSYS change a maximum of 3.852°C with the ANSYS simulation showing a slightly higher effectiveness. It can also be seen that the helium pressure drop in the ANSYS simulation is slightly lower than in the Flownex. This is due to the different wall functions used and ANSYS being more geometry sensitive than the Flownex. Overall the simulation comparison is good and the differences small.

HEAT EXCHANGER 2

Table 14: Heat exchanger 2 detailed Flownex parameters

Parameter	**Value**
Diameter Helium	0.00173 m
Diameter Solar Salt	0.00135 m
Flow Area Helium	0.351 m^2

Flow Area Solar Salt	0.214 m^2
Fluid Path Length	0.236 m
Plate thickness	0.0017 m
Heat transfer Area	382.761 m^2
Volume	0.609 m^3
Face Area	2.58 m^2
effectiveness	0.798
Number of Symmetry heat transfer elements	298524
Compact factor	628 m^{-1}
Pitch	0.0025 m
Helium Average Reynolds Number	1793.24
Solar Salt Average Reynolds Number	472.379

Figure 32 shows the cross section symmetry element design with units being in millimetre.

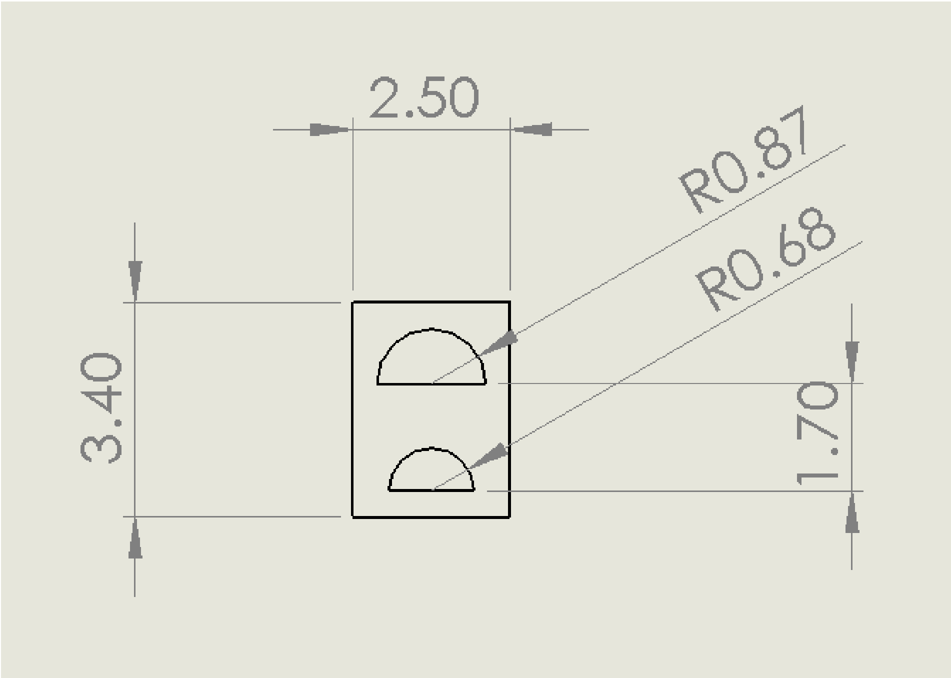

Figure 32: Heat exchanger 2 element

<u>ANSYS Fluent Results and discussion</u>

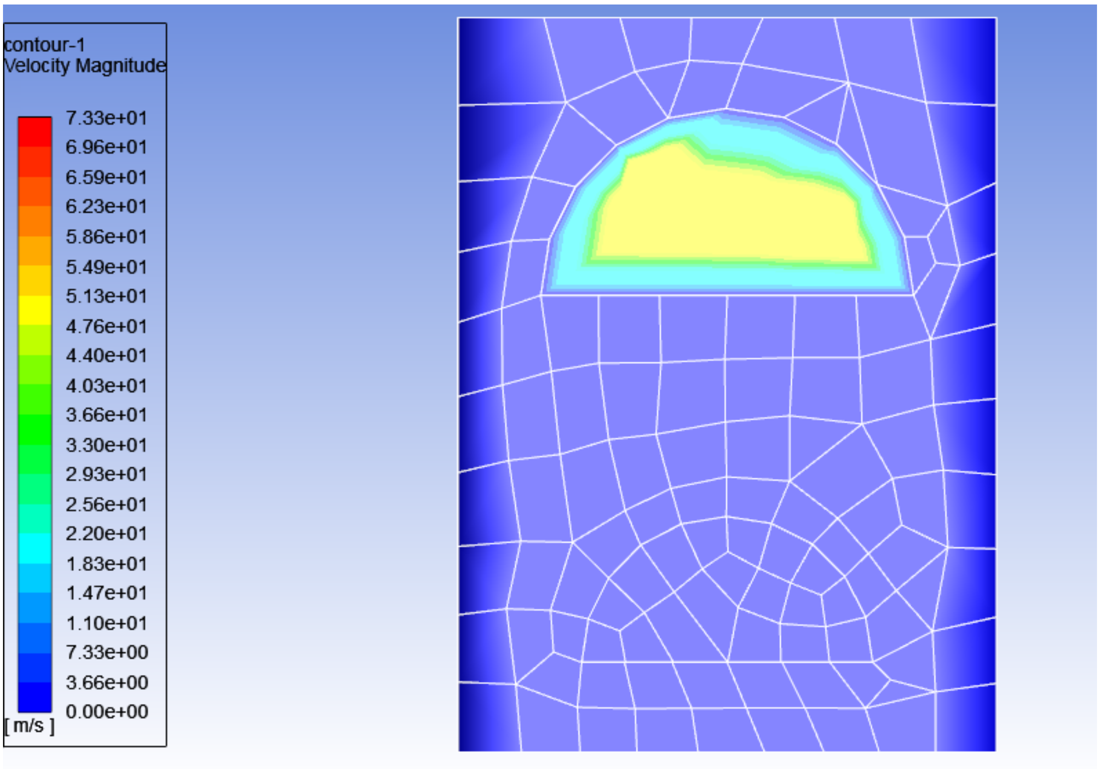

Figure 33: Heat exchanger 2 velocity magnitude

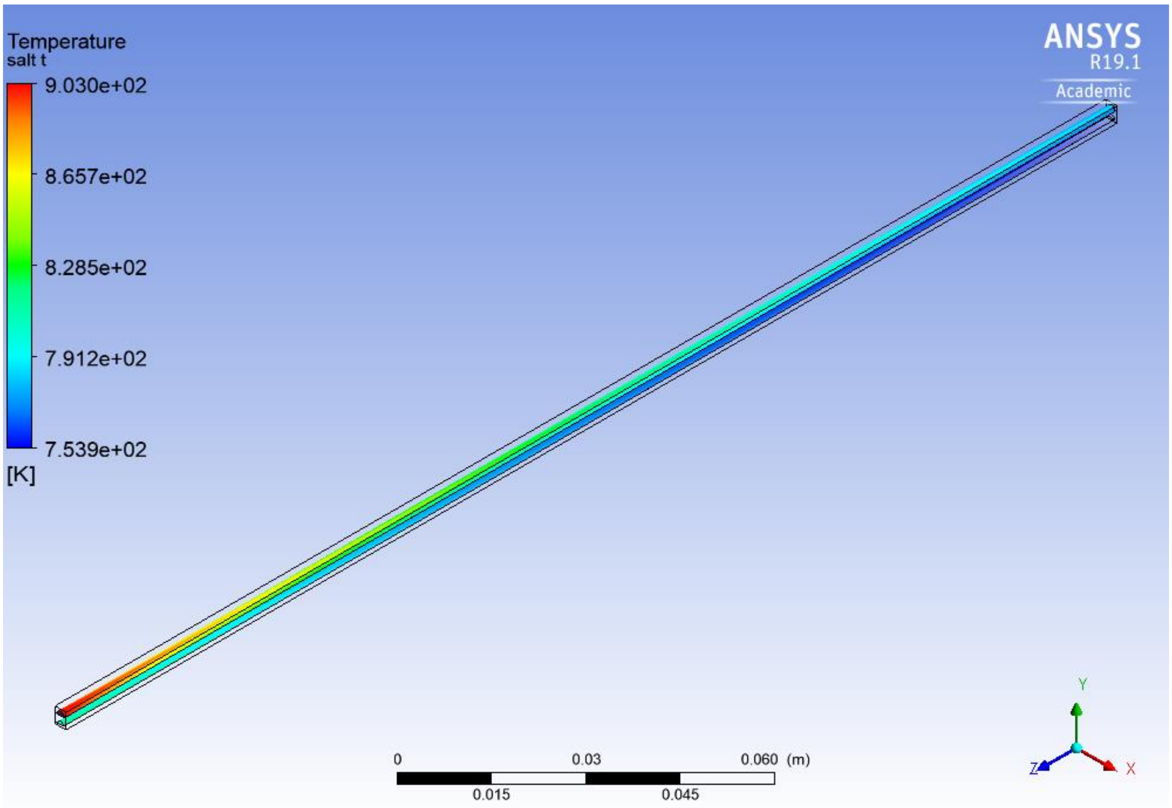

Figure 34: Heat exchanger 2 3D temperature profile

Figure 34 shows the temperature profile in the fluids and looks similar to heat exchanger 1. No irregularities are present and the temperature distributions within the streams are smooth. Figure 35 shows the fluid temperature along the length of the heat exchanger and follows a counter flow heat exchanger pattern.

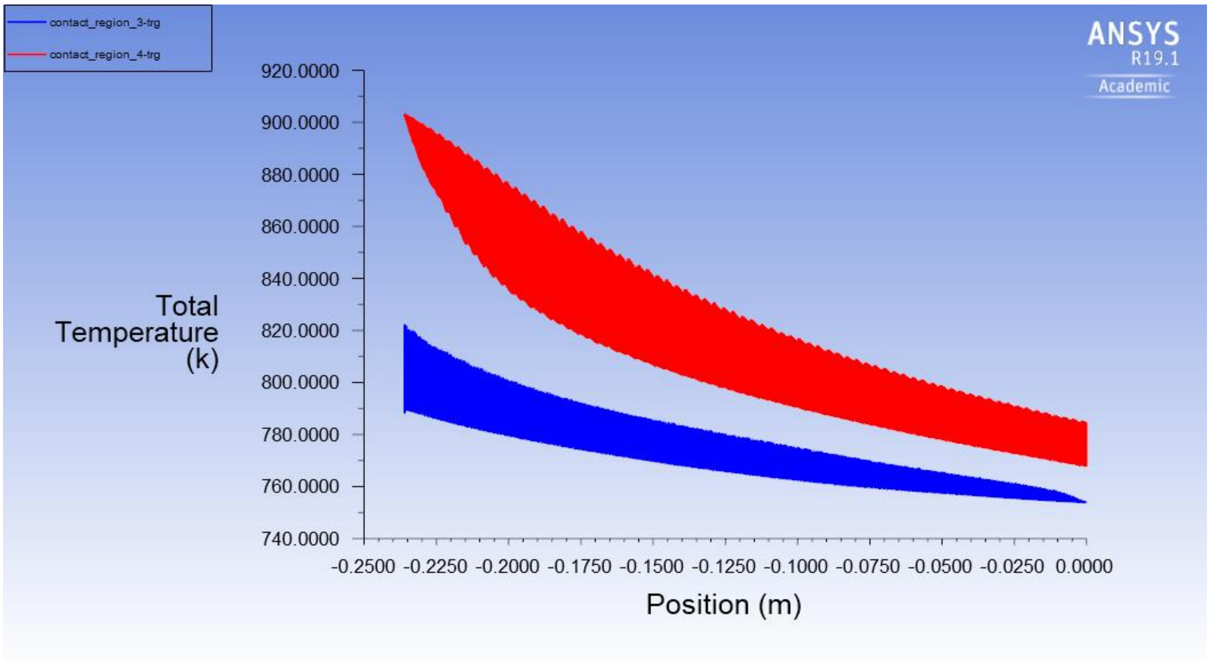

Figure 35: Heat exchanger 2 fluid temperature along the path length

Table 15: Heat exchanger 2 results comparison

Parameter	ANSYS Fluent	Flownex	Absolute Difference
Helium Inlet Temperature (°C)	630	630	0
Solar Salt Inlet Temperature (°C)	480.766	480.766	0
Helium Outlet Temperature (°C)	506.288	510.919	4.631
Solar Salt Outlet Temperature (°C)	523.707	518.334	5.373
Helium Pressure Drop (kPa)	12.72	14.917	2.197
Solar Salt Pressure Drop (kPa)	11.7	15.518	3.818
Effectiveness	0.829	0.798	0.031
Helium Inlet Density (kg/m^3)	1.26	1.26	0

Helium Outlet Density (kg/m^3)	1.45	1.44	0.01
Helium Inlet Velocity (m/s)	54.549	54.549	0
Helium Outlet Velocity (m/s)	47.519	47.68	0.161
Solar Salt Velocity (m/s)	0.636	0.636	0

The result comparison for heat exchanger 2 shows a maximum temperature difference of 5.373 °C and a maximum pressure drop difference of 3.818 kPa. The ANSYS simulation has a slightly higher effectiveness with an increase of 0.031 compared to the Flownex result.

HEAT EXCHANGER 3

Table 16: Heat exchanger 3 detailed Flownex parameters

Parameter	Value
Diameter Helium	0.00203 m
Diameter Solar Salt	0.00214 m
Flow Area Helium	0.351 m^2
Flow Area Solar Salt	0.391 m^2
Fluid Path Length	0.286 m
Plate thickness	0.002 m
Heat transfer Area	395.113 m^2
Volume	0.778 m^3
Face Area	2.726 m^2
Effectiveness	0.798

Number of Symmetry heat transfer elements	216811
Compact factor	507.773 m^{-1}
Pitch	0.003 m
Helium Average Reynolds Number	2104.32
Solar Salt Average Reynolds Number	410.309

Figure 36 shows the cross section symmetry element design with units being in millimetre.

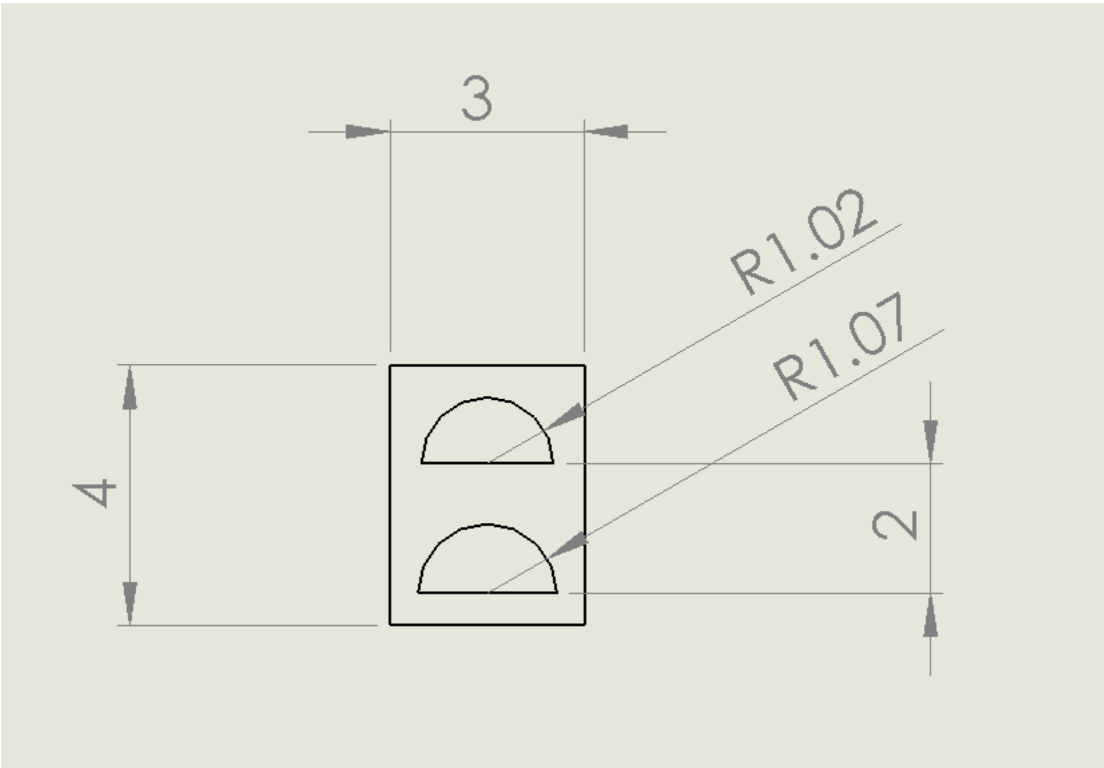

Figure 36: Heat exchanger 3 element

<u>ANSYS Fluent Results and discussion</u>

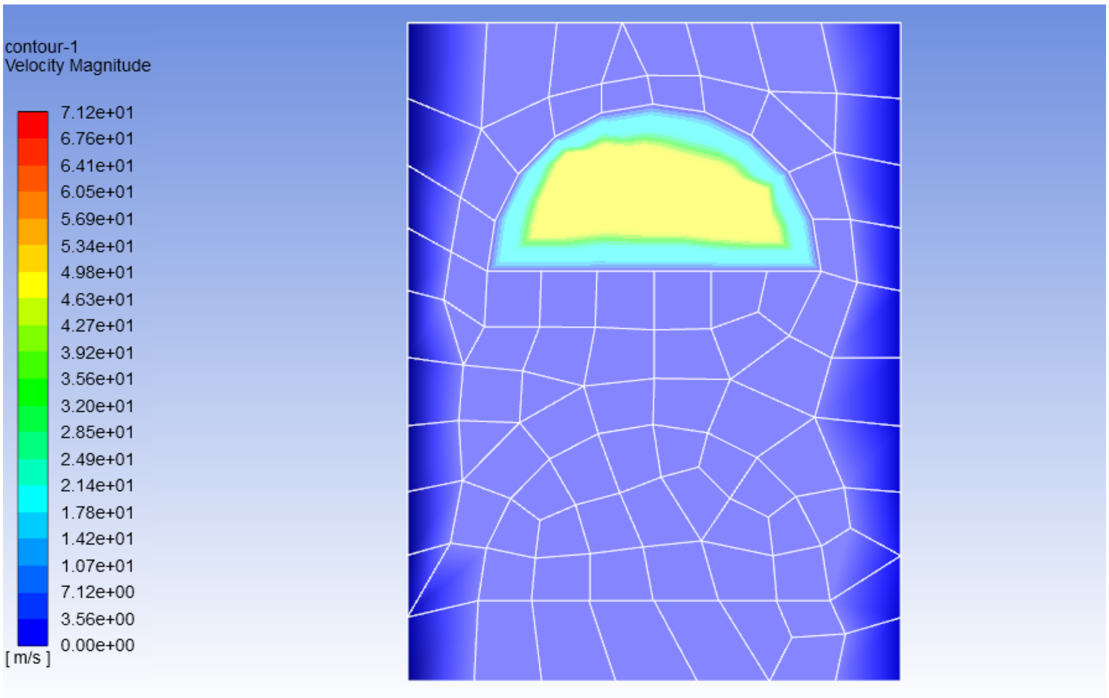

Figure 37: Heat exchanger 3 velocity magnitude

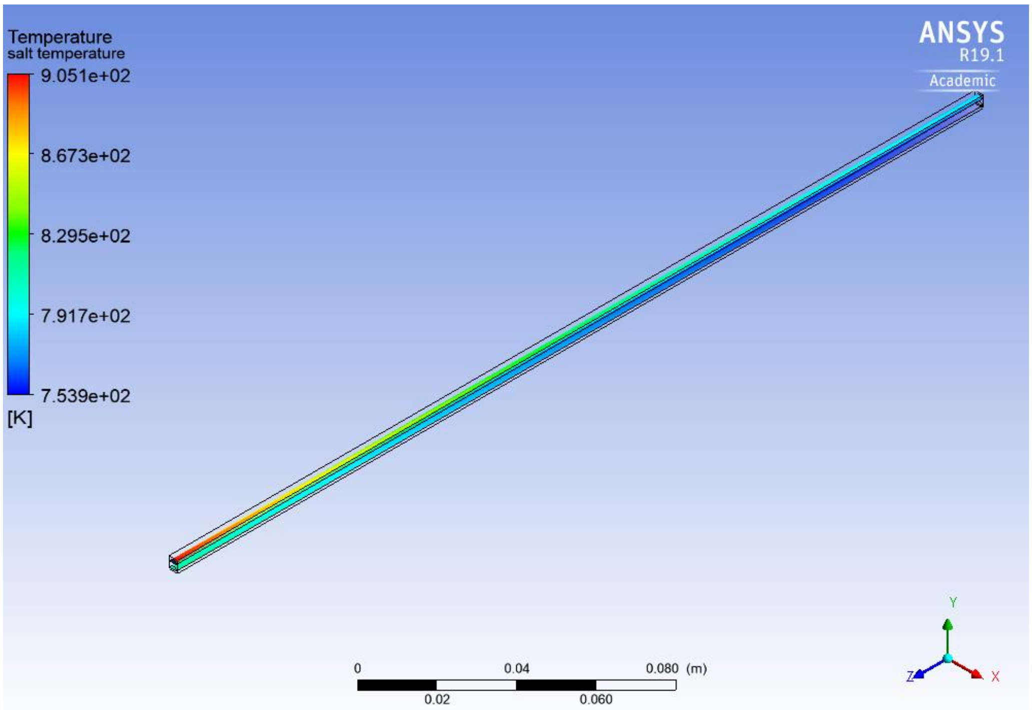

Figure 38: Heat exchanger 3, 3D temperature profile

Figure 38 shows the 3D representation of the heat exchanger temperatures. A similar result as the previous heat exchangers can be seen. Figure 39 shows similar results to the other heat exchangers and also follow a counter flow heat exchanger profile.

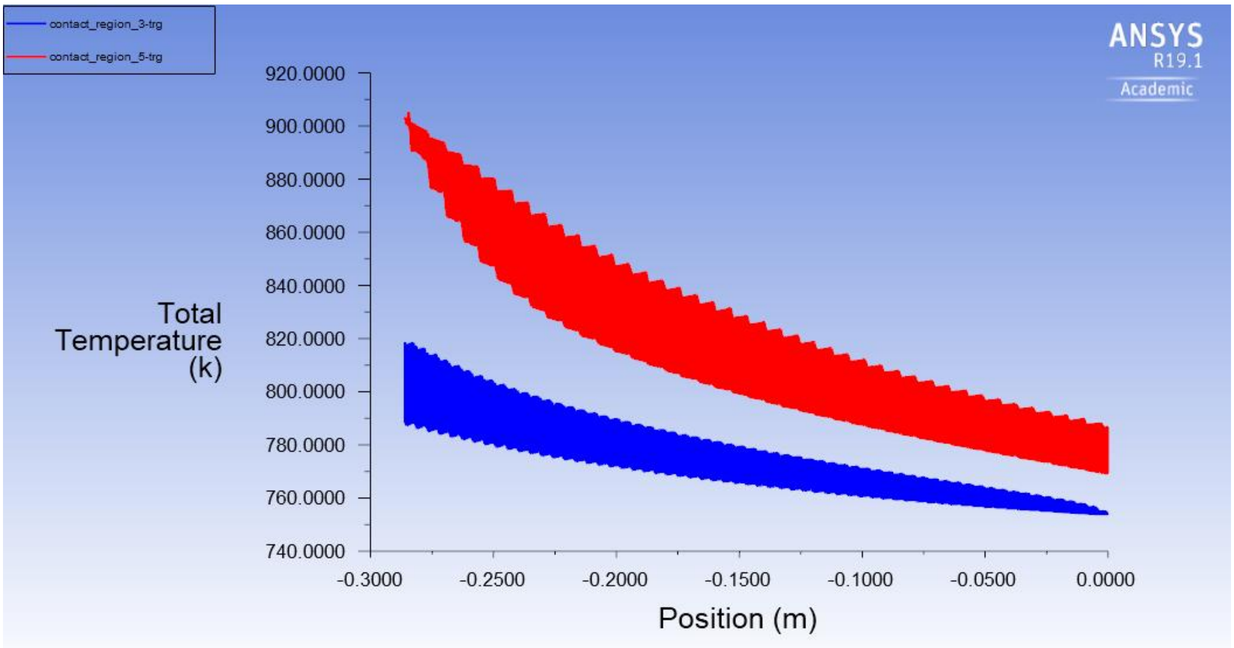

Figure 39: Heat exchanger 3 fluid temperature along the path length

Table 17: Heat exchanger 3 results comparison

Parameter	ANSYS Fluent	Flownex	Absolute Difference
Helium Inlet Temperature (°C)	630	630	0
Solar Salt Inlet Temperature (°C)	480.766	480.766	0
Helium Outlet Temperature (°C)	509.908	510.919	1.011
Solar Salt Outlet Temperature (°C)	523.629	518.334	5.295
Helium Pressure Drop (kPa)	10.65	13.086	2.436
Solar Salt Pressure Drop (kPa)	3.196	4.099	0.903
Effectiveness	0.805	0.798	0.007
Helium Inlet Density (kg/m^3)	1.26	1.26	0
Helium Outlet Density (kg/m^3)	1.44	1.44	0
Helium Inlet Velocity (m/s)	54.549	54.549	0
Helium Outlet Velocity (m/s)	47.752	47.644	0.108
Solar Salt Velocity (m/s)	0.349	0.349	0

The maximum temperature difference between the two simulations is 5.295 °C with the maximum pressure drop difference being 2.436 kPa. The effectiveness of the two simulations are similar with a small difference of 0.007.

HEAT EXCHANGER 4

Table 18: Heat exchanger 4 detailed Flownex parameters

Parameter	Value
Diameter Helium	0.00165 m
Diameter Solar Salt	0.00219 m
Flow Area Helium	0.286 m^2
Flow Area Solar Salt	0.504 m^2
Fluid Path Length	0.214 m
Plate thickness	0.0016 m
Heat transfer Area	296.117 m^2
Volume	0.597 m^3
Face Area	2.79 m^2
Effectiveness	0.798
Number of Symmetry heat transfer elements	267401
Compact factor	496.14 m^{-1}
Pitch	0.0032 m
Helium Average Reynolds Number	2099.49
Solar Salt Average Reynolds Number	325.085

Figure 40 shows the cross section symmetry element design with units being in millimetre.

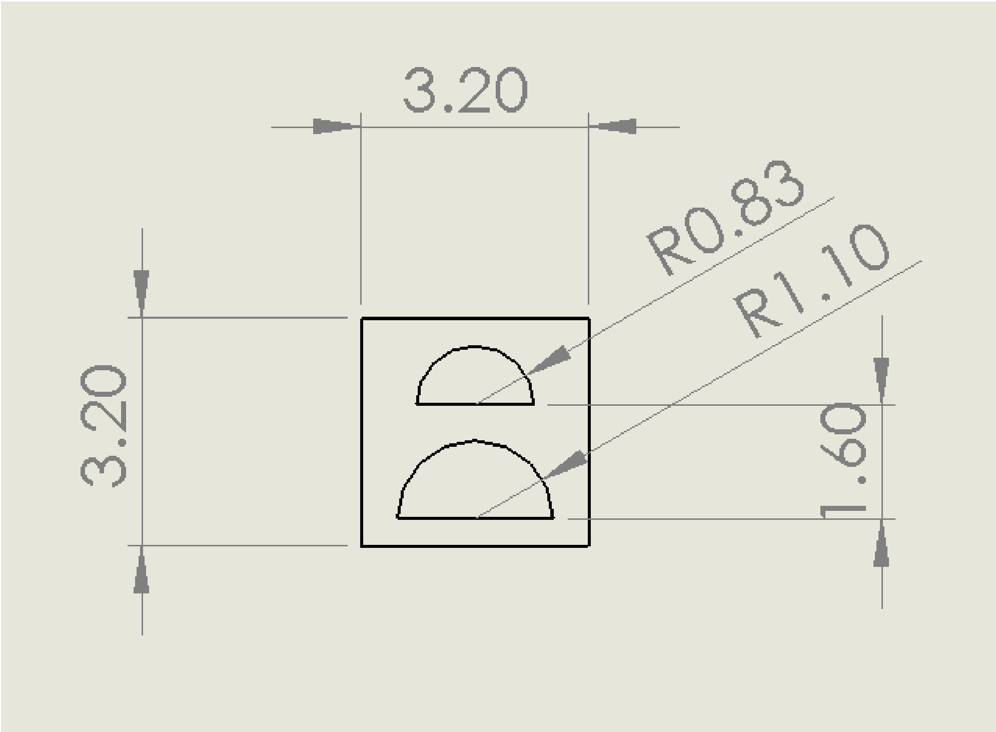

Figure 40: Heat exchanger 4 element

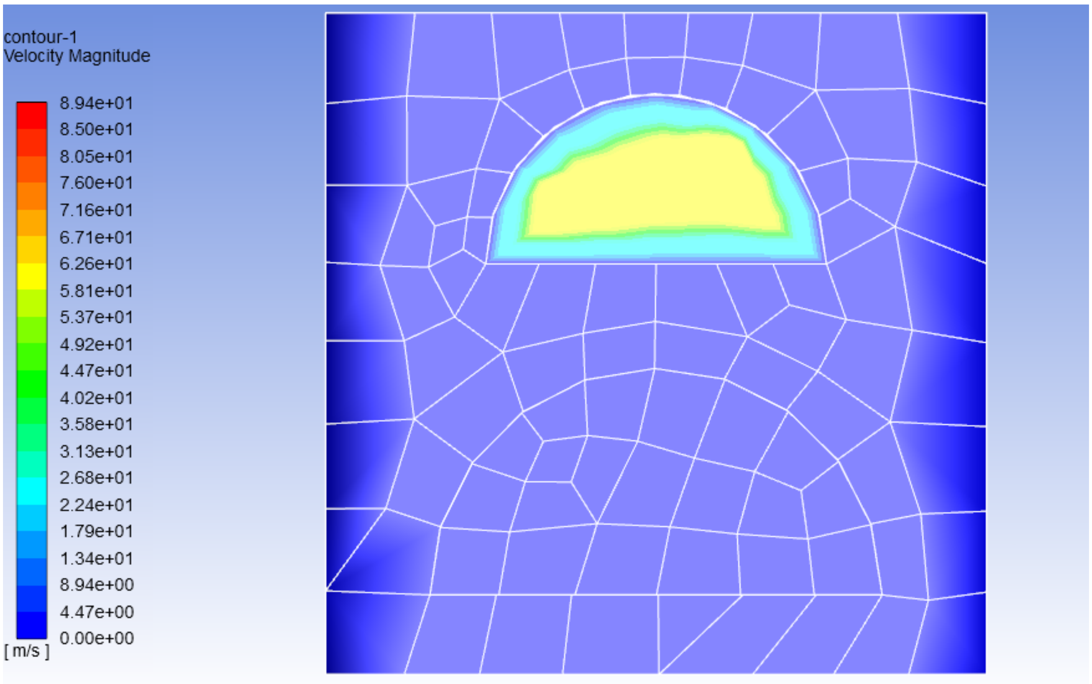

Figure 41: Heat exchanger 4 velocity magnitude

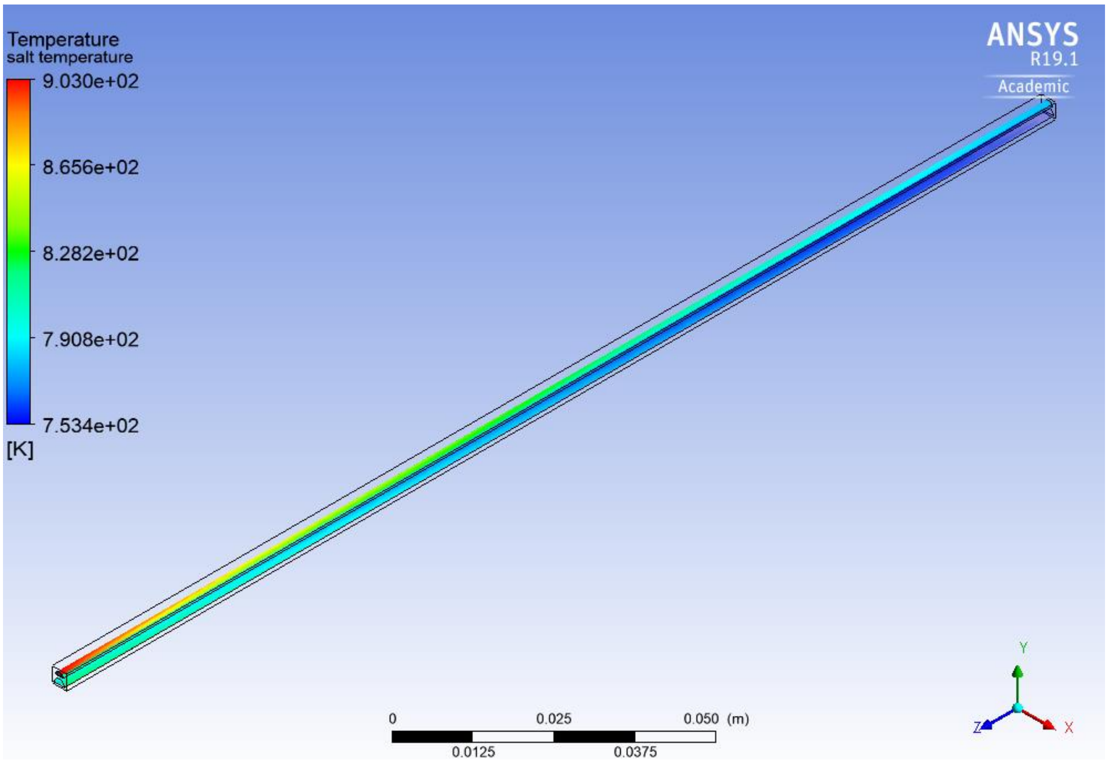

Figure 42: Heat exchanger 4, 3D temperature profile

The results displayed in Figure 42 and Figure 43 is similar to the other simulations results. The temperature profile follows the expected curve of a counter-flow heat exchanger.

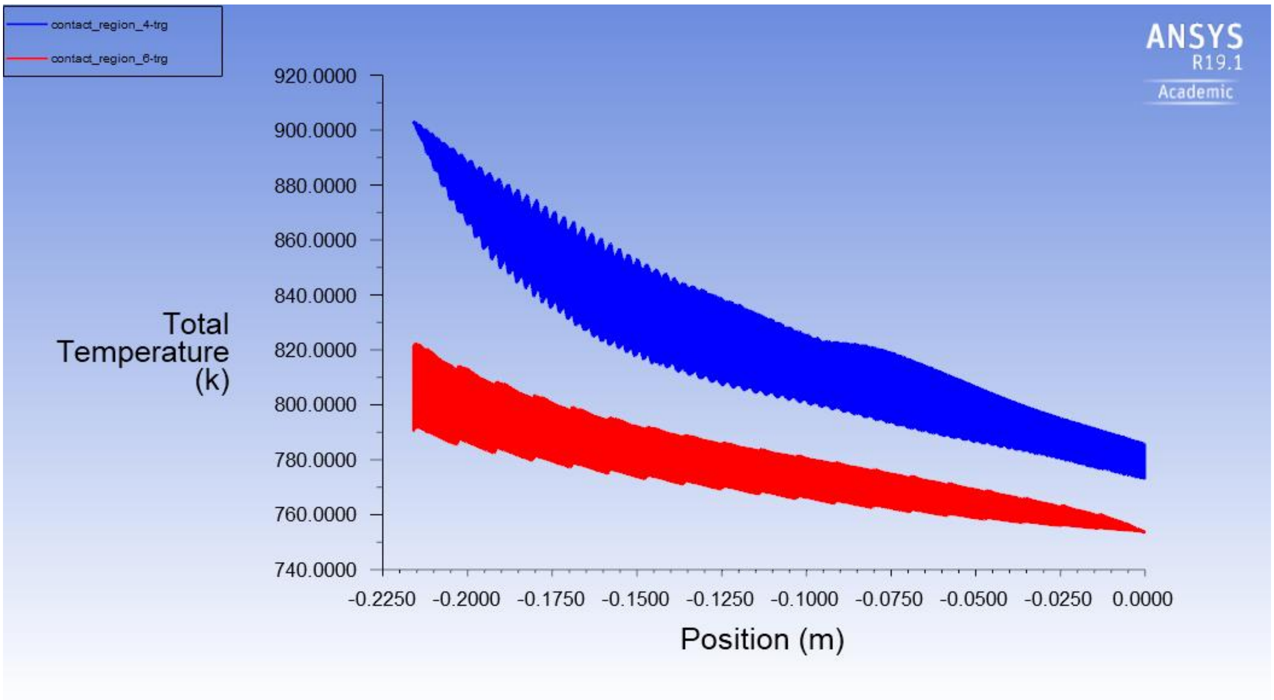

Figure 43: Heat exchanger 4 fluid temperature along the path length

Table 19: Heat exchanger 4 results comparison

Parameter	ANSYS Fluent	Flownex	Absolute Difference
Helium Inlet Temperature (°C)	630	630	0
Solar Salt Inlet Temperature (°C)	480.766	480.766	0
Helium Outlet Temperature (°C)	508.025	510.919	2.894
Solar Salt Outlet Temperature (°C)	525.283	518.334	6.949
Helium Pressure Drop (kPa)	15.9	18.170	2.27

Solar Salt Pressure Drop (kPa)	1.8	2.265	0.465
Effectiveness	0.818	0.798	0.02
Helium Inlet Density (kg/m^3)	1.26	1.26	0
Helium Outlet Density (kg/m^3)	1.46	1.44	0.02
Helium Inlet Velocity (m/s)	66.962	66.962	0
Helium Outlet Velocity (m/s)	58.417	58.61	0.193
Solar Salt Velocity (m/s)	0.270	0.270	0

The maximum temperature difference in the two simulations is 6.949 °C with the maximum pressure drop difference being 2.27 kPa. The effectiveness has a difference of 0.02. These differences are larger than the other simulations.

HEAT EXCHANGER 5

Table 20: Heat exchanger 5 detailed Flownex parameters

Parameter	**Value**
Diameter Helium	0.00196 m
Diameter Solar Salt	0.00233 m
Flow Area Helium	0.335 m^2
Flow Area Solar Salt	0.473 m^2
Fluid Path Length	0.267 m
Plate thickness	0.002 m
Heat transfer Area	364.83 m^2
Volume	0.782 m^3
Face Area	2.93 m^2
effectiveness	0.798
Number of Symmetry heat transfer elements	221972
Compact factor	466.33 m^{-1}
Pitch	0.0034 m
Helium Average Reynolds Number	2128.896
Solar Salt Average Reynolds Number	368.087

Figure 44 shows the cross section symmetry element design with units being in millimetre.

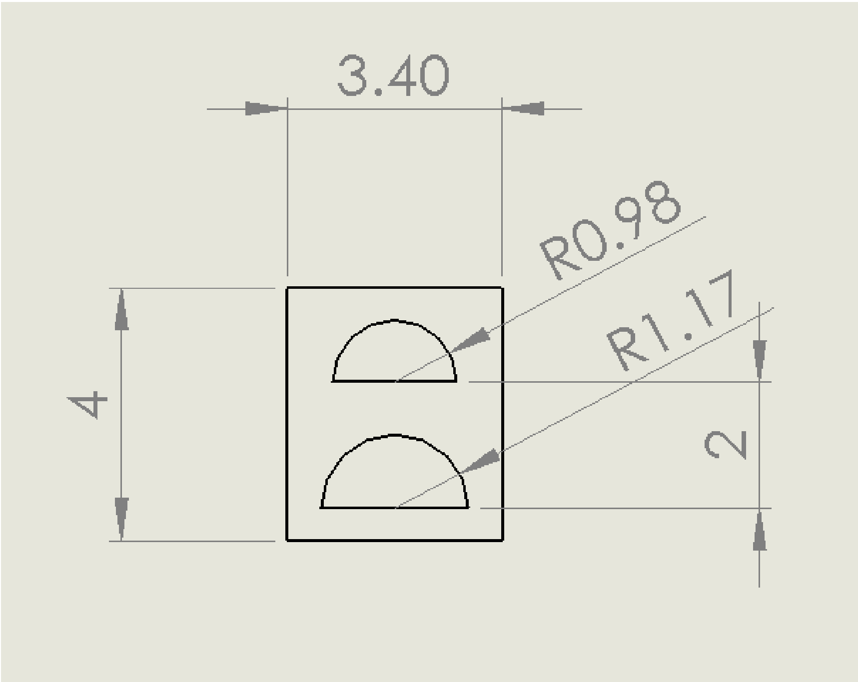

Figure 44: Heat exchanger 5 element

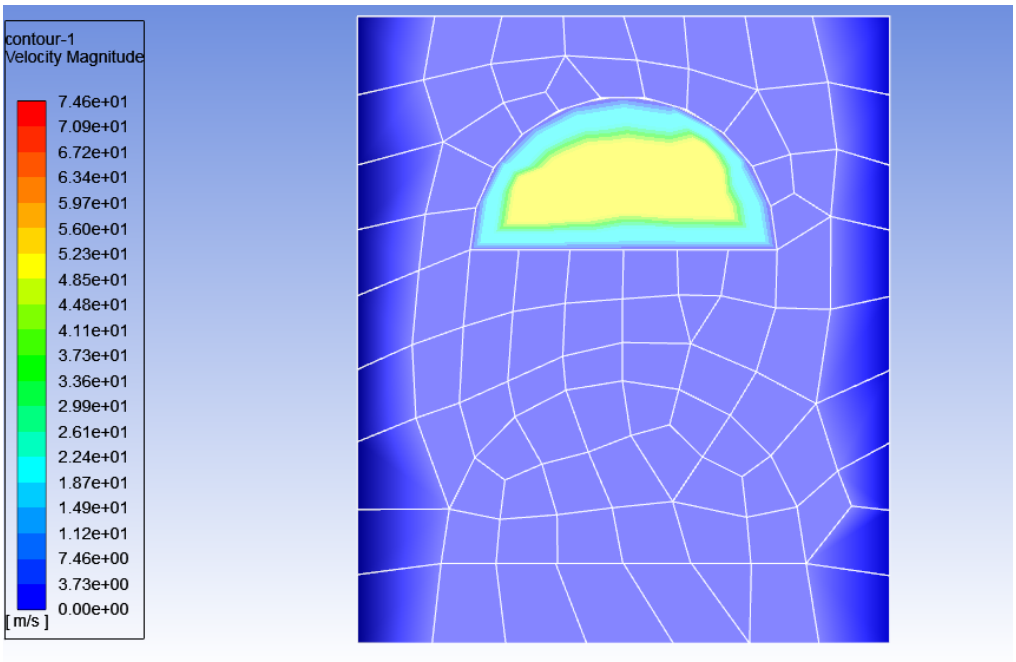

Figure 45: Figure 41: Heat exchanger 5 velocity magnitude

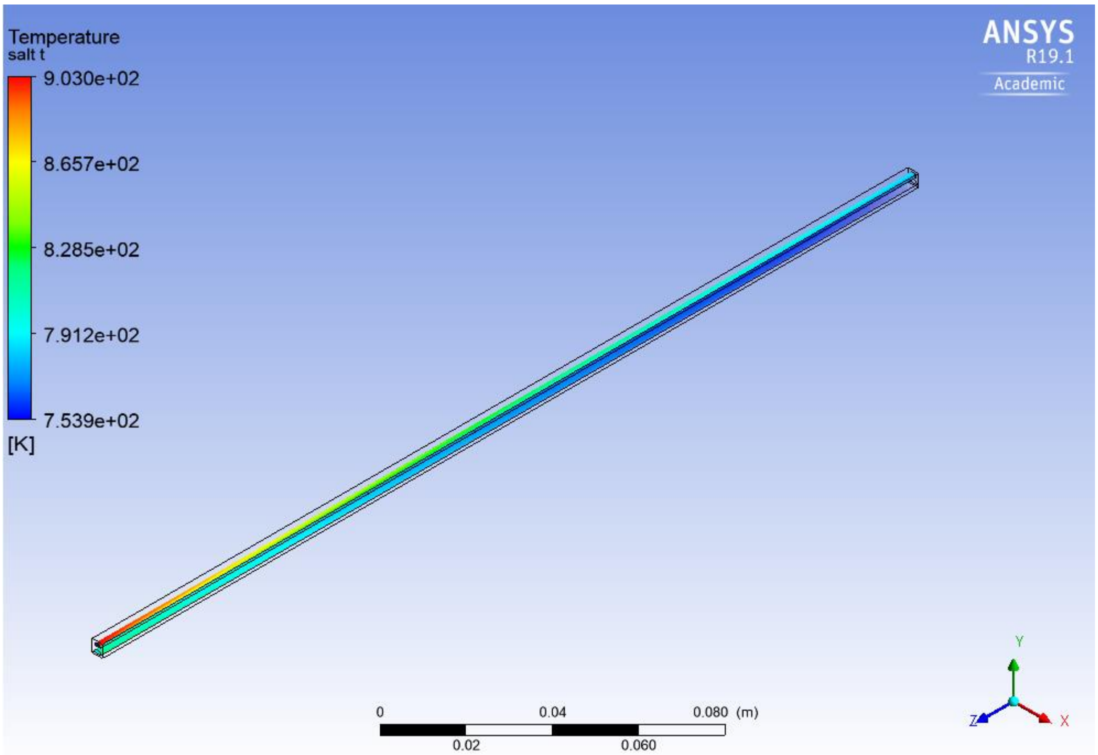

Figure 46: Heat exchanger 5, 3D temperature profile

Figure 46 and Figure 47 show similar results to the other simulations and follows the expected temperature curve of a counter flow heat exchanger.

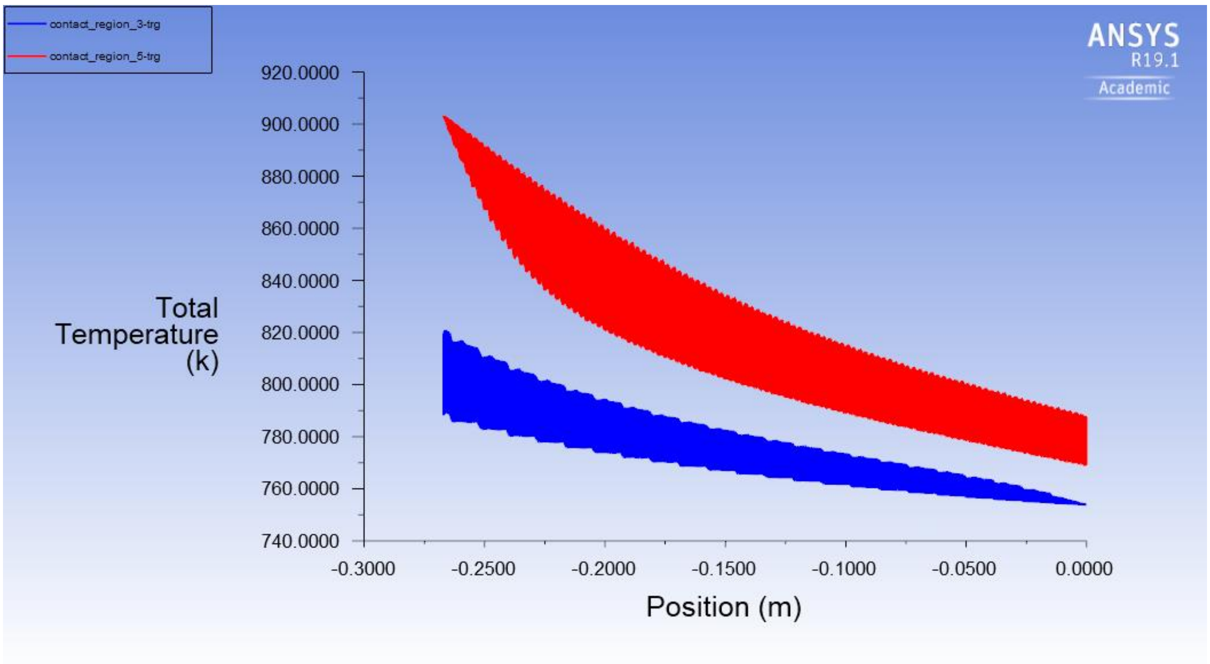

Figure 47: Heat exchanger 5 fluid temperature along the path length

Table 21: Heat exchanger 5 results comparison

Parameter	ANSYS Fluent	Flownex	Absolute Difference
Helium Inlet Temperature (°C)	630	630	0
Solar Salt Inlet Temperature (°C)	480.766	480.766	0
Helium Outlet Temperature (°C)	510.519	510.886	0.367
Solar Salt Outlet Temperature (°C)	523.603	518.334	5.269
Helium Pressure Drop (kPa)	11.08	13.729	2.649
Solar Salt Pressure Drop (kPa)	2.073	2.661	0.588
effectiveness	0.80	0.798	0.002
Helium Inlet Density (kg/m^3)	1.26	1.26	0
Helium Outlet Density (kg/m^3)	1.44	1.44	0
Helium Inlet Velocity (m/s)	57.16	57.16	0
Helium Outlet Velocity (m/s)	50.07	49.94	0.13
Solar Salt Velocity (m/s)	0.287	0.287	0

The largest temperature difference between the two simulations is 5.269 °C and the largest pressure drop difference is 5.269 kPa. The effectiveness of both simulations differs with 0.002.

Final Design selection

From the results obtained from the simulation heat exchanger 3 is selected to be the final design based on the following arguments.

- The total volume of heat exchanger 3 is below 1 m^3 .The small volume will reduce the cost of the heat exchanger and will ensure that there is enough space in the reactor assembly.

- Heat exchanger 3 shows pressure drops well below the allowed pressure drop for both fluid streams.

- Heat exchanger 3 might have a slightly higher volume, but will be more practical to implement in the reactor assembly due to its small face area.

- Heat exchanger 3 showed the best result comparison between the two simulation programs.

8. DETAILED DESIGN

The length, pitch, plate thickness and fluid diameters are known as the values for heat exchanger 3 are used. From the literature plate configuration a) is chosen with a length to width ratio of roughly 2.3. This will give the same results as a sole counter-flow configuration based on the data from (Son, Lee et al. 2015).

The plates for a single heat exchanger block can therefore be designed with a length to width ratio of roughly 2.3. The height of the heat exchanger is limited to the reactor design and is chosen as 1.3 m as indicated in Figure 19.

Figure 48 and Figure 49 show the final plate design for the IHX with the units being in millimetre. These plates are stacked and diffusion bonded to each other to form the heat exchanger block.

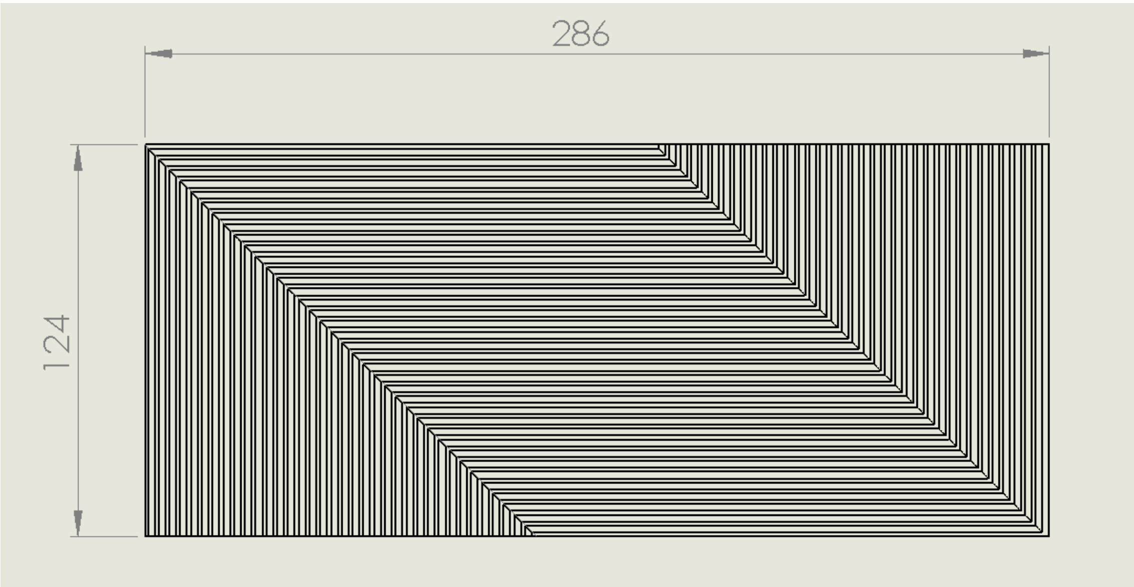

Figure 48: Salt Plate Final Design

Figure 49: Helium Plate Final Design

AHTR Assembly

With the height chosen as 1.3 m the plates can be assembled to reach the desired flow area and heat transfer area. In order to reach the desired specifications 17 of these stacked plate assemblies are required to reach the total heat transfer and flow areas. In the final design 18 heat exchangers are assembled around the power generating unit as seen in Figure 52.

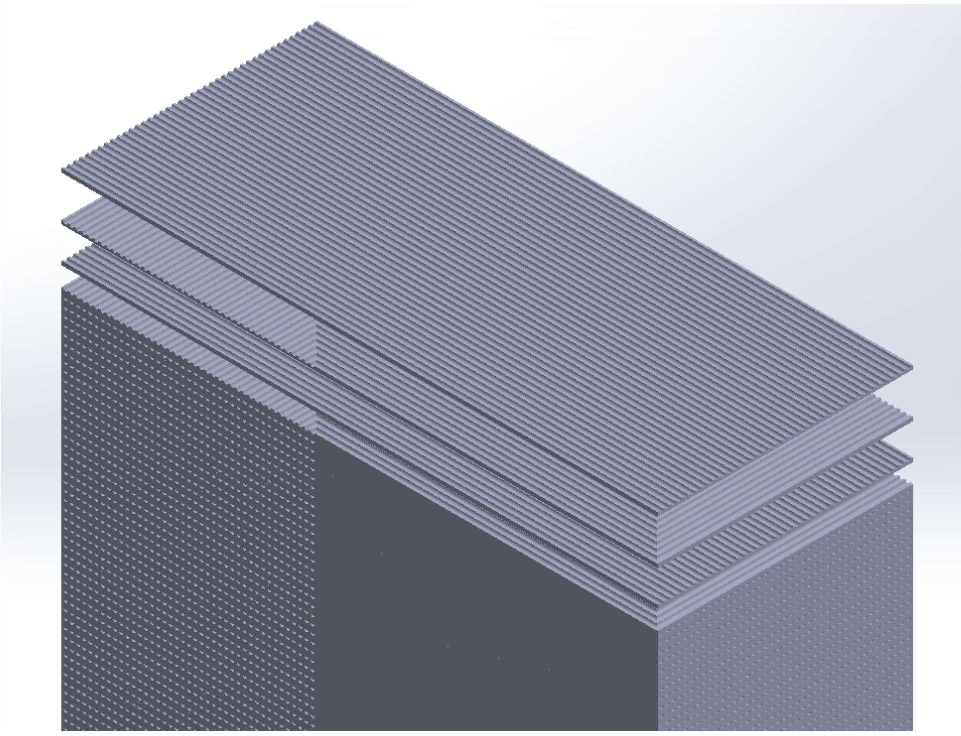

Figure 50: Plate Assembly Exploded view

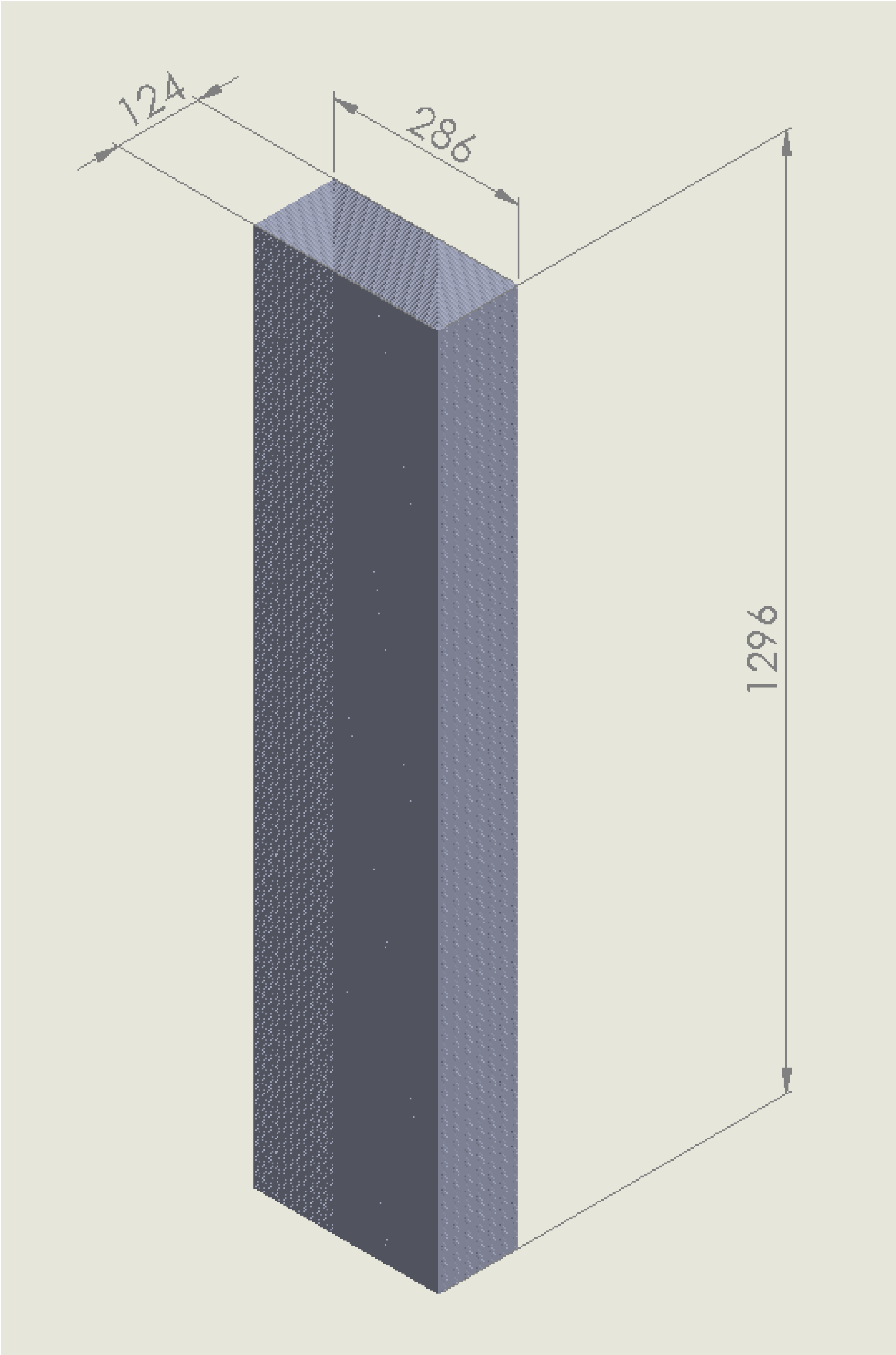

Figure 51: Stacked Plate Assembly (mm)

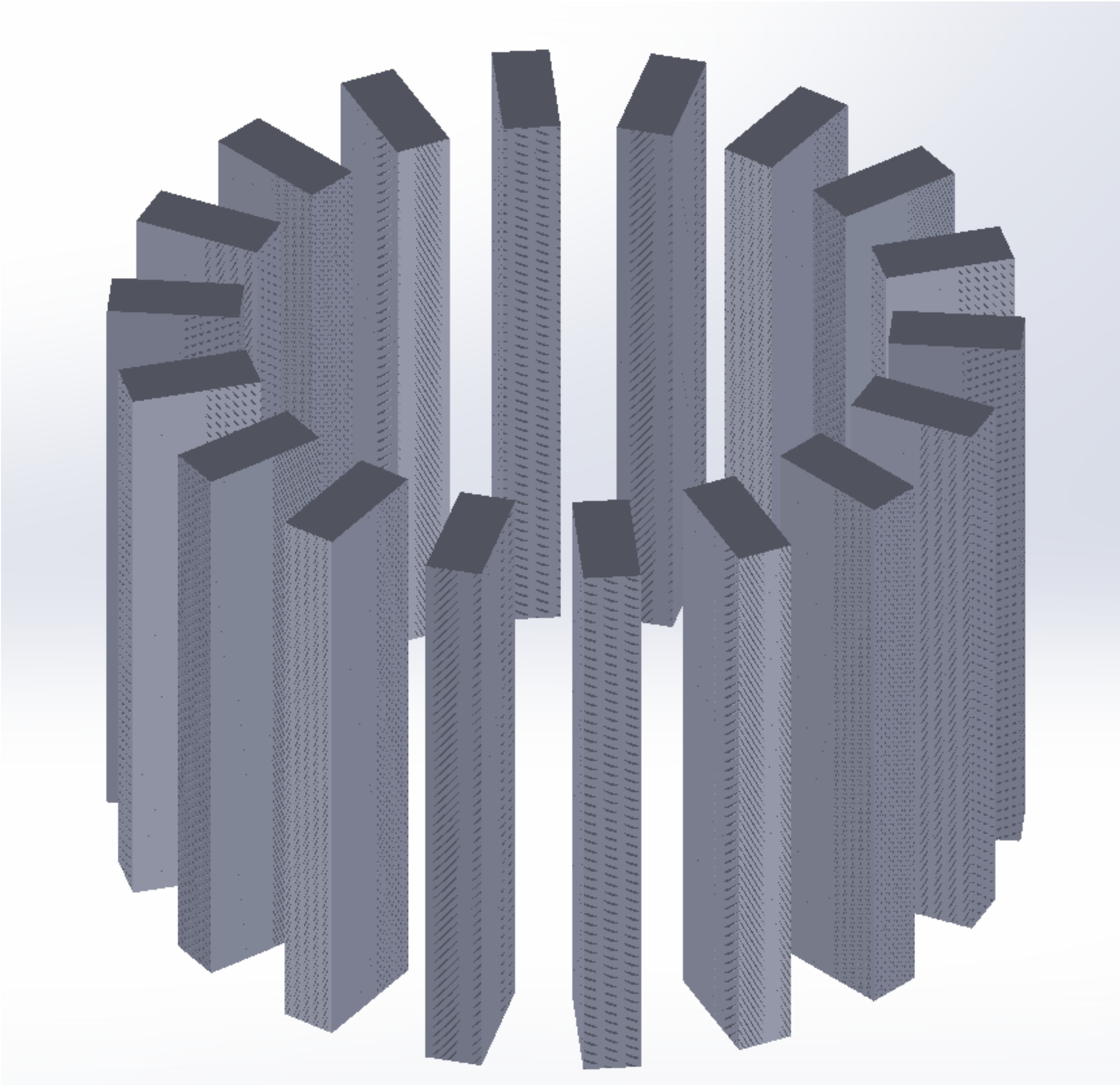

Figure 52: Heat exchanger assembly

Advantages of multiple heat exchanger design:

- Easier assembly due to the smaller size of each individual heat exchanger.
- More control in the heat exchange by controlling valves to each heat exchanger.
- Maintenance can be done by removing one heat exchanger at a time without stopping the reactor. This is also the main reason why 18 heat exchangers are used in the assembly.

Transient simulations during operating

The IHX consists of several separate heat exchangers assembled around the reactor as seen in Figure 52. The total effectiveness of the IHX can be controlled by individually controlling valves at the inlets of each heat exchanger unit. In order to see how the effectiveness, temperatures and pressure drops changes with the valve controlling method a transient simulation is done in Flownex.

During operation the mass flows and the inlet conditions are kept constant. If the flow through a heat exchanger unit is closed by a valve it would only affect the total flow area of the fluids. The change in flow area would change the velocity at the inlets, and therefore the heat transfer and the pressure drops.

Simulation Setup:

- The final IHX design parameters are used in the Flownex model.
- The total flow area for a single heat exchanger unit is calculated.
- A variable is assigned to the Flownex model to control the amount of heat exchanger blocks that is being used. The total flow area would then be the amount of heat exchanger blocks in use, multiplied by the flow area of one heat exchanger block.
- At the start of the simulation all 18 heat exchanger blocks are in operation.
- Every 20 seconds one heat exchanger is closed until there are only 10 heat exchanger blocks in operation.

Results

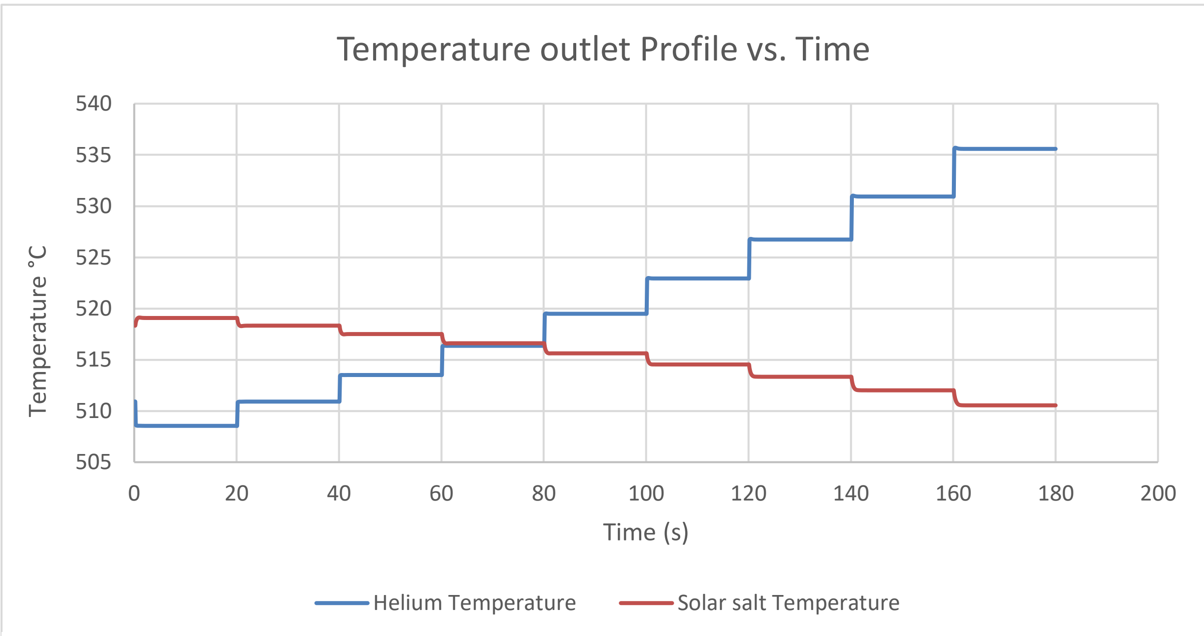

Figure 53: Temperature Profile vs. Time

At time 0 to 20 there are 18 heat exchanger blocks in operation, decreasing by 1 every 20 seconds. As less heat exchanger blocks are used, the helium temperature rises and the solar salt temperature drops. From the results it is clear that the temperature can be successfully controlled by controlling the inlet valves to the several heat exchanger blocks.

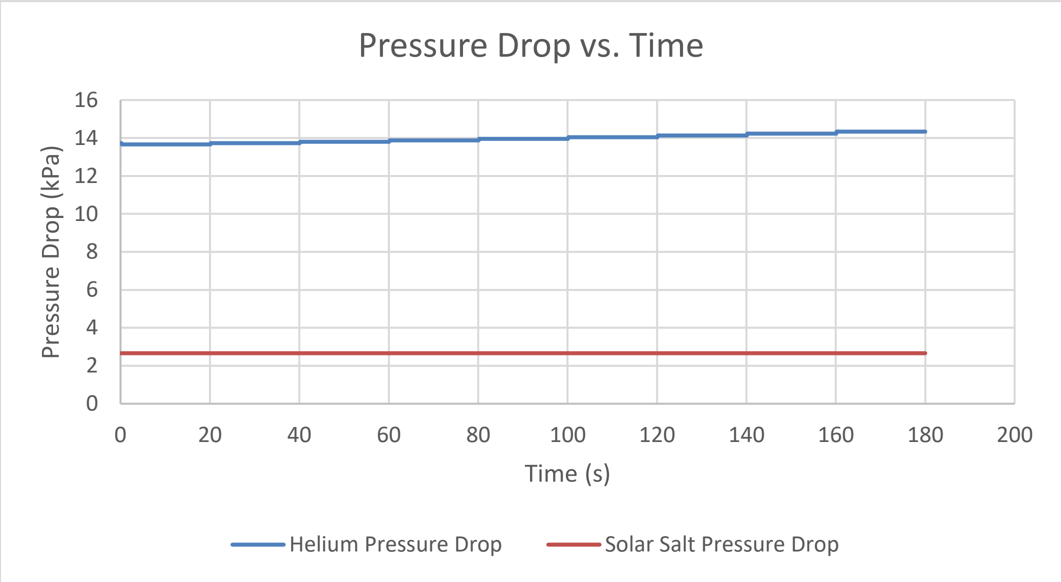

Figure 54: Pressure Drop vs. Time

At time 0 to 20 there are 18 heat exchanger blocks in operation, decreasing by 1 every 20 seconds. The pressure drop in both fluids streams are not sensitive to the amount of heat exchanger blocks in operation. A small increase in pressure drop is seen in the helium. This is due to the increased flow velocity that occurs when the total flow area is decreased.

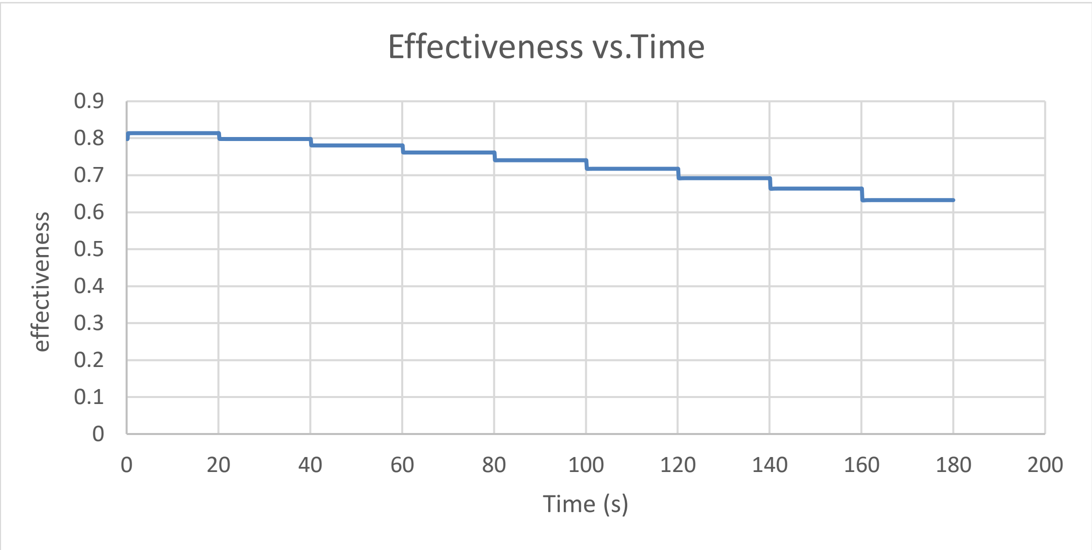

Figure 55: Effectiveness vs. Time

As expected the effectiveness decreases as the amount of heat exchanger blocks in operation decreases. It can be seen that between 20 and 40 seconds when 17 heat exchanger blocks are in use, the effectiveness is 0.798 as it should be.

This method of temperature control could be used during the reactor startup or during accident conditions to ensure that the temperatures stay in an acceptable range.

9. CONCLUSION

The Eskom AHTR has the potential to form part of the next generation smart electricity grid by implementing a load following capability through molten salt heat storage. The heat generated in the reactor is transferred to high pressure helium where and intermediate heat exchanger transfers the heat to molten salt. The intermediate heat exchanger required for the AHTR will operate under unique conditions and requires a design so that materials and types of heat exchangers can be tested. Solar salt is used as the heat storage medium as it is a proven technology with minimal corrosion effects. There are however other options for thermal storage involving molten salt with higher operating temperatures. Data is required in order to test the feasibility of other molten salts.

From the literature several types of heat exchangers are looked at as potential designs for the IHX. A printed circuit heat exchanger design is chosen due to its high compactness and capability of handling large pressure differentials in the fluids. Hastelloy N is chosen as the heat exchanger material as it has a high corrosive resistance and acceptable design stresses at the operating temperatures and pressures. Hastelloy N can be diffusion bonded and therefore compatible with the manufacturing process of a printed circuit heat exchanger. Other materials would also be acceptable for the design; however more data is required in order to do a feasibility analysis with corrosion being the largest factor in the heat exchanger lifetime.

The scoping of the heat exchanger is done in an EES code and gives a rough indication on the specifications of the heat exchanger. The results from the scope are used in a Flownex where the length, flow areas and hydraulic diameters are varied in a Monte Carlo sensitivity analysis for 5000 iterations. From the Flownex results, 5 heat exchangers are chosen that match the criteria for the IHX design. The chosen 5 heat exchangers are optimized and simulated in ANSYS Fluent and the results where compared to the Flownex results. The solutions from both simulation programs showed similar results with small discrepancies in the element properties.

From the 5 heat exchangers 1 was chosen that would be most suitable for the AHTR. The selected heat exchanger consists of 18 heat exchanger blocks with specifications illustrated in the final design section. With the heat exchanger divided into separate units, the effectiveness can be controlled by controlling valves at the inlets of these heat exchanger blocks. A transient simulation in Flownex illustrates the control of temperatures during the operation of the AHTR and shows that the designed heat exchanger can successfully handle the heat load that is required.

The problem states that the intermediate heat exchanger required for the AHTR requires a compact novel design to successfully operate within the unique thermal, pressure and chemical conditions it is subjected to while successfully handling the heat load required for the AHTR as efficiently as possible.

The final design in this study can handle the thermal, pressure and chemical conditions. This was done by selecting a material that fit the requirements as well as adjusting the mechanical design to ensure an allowable stress within the material. The heat load and efficiency of the heat exchanger was designed and optimized in Flownex. From this study a successful solution to the problem was achieved.

FUTURE WORK

From the literature and design considerations encountered in this study future work is identified before the design can be approved.

- The design needs to be tested. A smaller model operating under the exact same boundary conditions is required to fully verify the design.
- More data is required from different materials and their behaviour in molten salts to calculate their feasibility. The data is also required to create an ASME code case for materials in nuclear molten salt systems. The National Nuclear Regulator has strict requirements for approving designs, and sufficient data is essential.
- If the design model is verified, the rest of the heat exchangers in the AHTR can be designed and integrated into the reactor assembly.
- Different header mountings for the heat exchanger block should be considered to ensure minimal losses.

ACKNOWLEDGMENTS

I would like to acknowledge Prof. A.C. Cilliers for his assistance in concept design as well as his leadership within the AHTR Research and development team. Roelf Laurens, Marinus Potgieter and Bennie du Toit for assistance in the Flownex modelling.

10. REFERENCES

Aquaro, D. and M. J. A. T. E. Pieve (2007). "High temperature heat exchangers for power plants: Performance of advanced metallic recuperators." **27**(2-3): 389-400.

Carling, R. and R. Bradshaw (1986). Review of the characterization of molten nitrate salt for solar central receiver applications. Intersociety energy conversion engineering conference. 21.

Chen, M., et al. (2016). "Pressure drop and heat transfer characteristics of a high-temperature printed circuit heat exchanger." **108**: 1409-1417.

Cheng, H., et al. (2018). "In situ synthesis and mechanism of mullite-silicon carbide composite ceramics for solar thermal storage." Ceramics International.

Fend, T., et al. (2011). "Experimental investigation of compact silicon carbide heat exchangers for high temperatures." International Journal of heat and mass transfer **54**(19-20): 4175-4181.

Fernandez, A., et al. (2012). "Molten salt corrosion of stainless steels and low-Cr steel in CSP plants." Oxidation of metals **78**(5-6): 329-348.

Fernández, I. and L. Sedano (2013). "Design analysis of a lead–lithium/supercritical CO2 Printed Circuit Heat Exchanger for primary power recovery." Fusion Engineering and Design **88**(9-10): 2427-2430.

Fox, M. (2017). Design Layout of the Eskom AHTR Reactor.

Hesselgreaves, J. E., et al. (2016). Compact heat exchangers: selection, design and operation, Butterworth-Heinemann.

Katoh, Y., et al. (2014). "Current status and recent research achievements in SiC/SiC composites." Journal of Nuclear Materials **455**(1): 387-397.

Kays, W. M. and A. L. London (1984). "Compact heat exchangers."

Kearney, D., et al. (2004). "Engineering aspects of a molten salt heat transfer fluid in a trough solar field." Energy **29**(5-6): 861-870.

Khare, S., et al. (2012). "Selection of materials for high temperature latent heat energy storage." Solar Energy Materials and Solar Cells **107**: 20-27.

Kruizenga, A. and D. Gill (2014). "Corrosion of iron stainless steels in molten nitrate salt." Energy Procedia **49**: 878-887.

Lee, Y. and J. I. Lee (2014). "Structural assessment of intermediate printed circuit heat exchanger for sodium-cooled fast reactor with supercritical CO2 cycle." Annals of Nuclear Energy **73**: 84-95.

Liu, B., et al. (2017). "Corrosion behavior of Ni-based alloys in molten NaCl-CaCl2-MgCl2 eutectic salt for concentrating solar power." Solar Energy Materials and Solar Cells **170**: 77-86.

McConohy, G. and A. Kruizenga (2014). "Molten nitrate salts at 600 and 680°C: Thermophysical property changes and corrosion of high-temperature nickel alloys." Solar Energy **103**: 242-252.

Mitchell, M. N. and K. Smit (2006). "Materials selection for advanced high temperature gas cooled reactors." Energy Materials **1**(3): 171-178.

Natesan, K., et al. (2009). "Preliminary issues associated with the next generation nuclear plant intermediate heat exchanger design." Journal of Nuclear Materials **392**(2): 307-315.

Patel, N. S., et al. (2017). "High-Temperature Corrosion Behavior of Superalloys in Molten Salts – A Review." Critical Reviews in Solid State and Materials Sciences **42**(1): 83-97.

Pizzolato, A., et al. (2017). "CSP plants with thermocline thermal energy storage and integrated steam generator–Techno-economic modeling and design optimization." **139**: 231-246.

Sabharwall, P., et al. (2014). "Advanced heat exchanger development for molten salts." Nuclear Engineering and Design **280**: 42-56.

Sabharwall, P., et al. (2011). "Evaluation metrics for intermediate heat exchangers for next generation nuclear reactors." Transactions of the American Nuclear Society **104**: 995.

Schulte-Fischedick, J., et al. (2007). "An innovative ceramic high temperature plate-fin heat exchanger for EFCC processes." Applied Thermal Engineering **27**(8-9): 1285-1294.

Sohal, M. S., et al. (2010). "Engineering database of liquid salt thermophysical and thermochemical properties." Idaho National Laboratory, Idaho Falls.

Son, S., et al. (2015). "Development of an advanced printed circuit heat exchanger analysis code for realistic flow path configurations near header regions." International Journal of heat and mass transfer **89**: 242-250.

Storm, P. C. (2017). Preliminary Design of Thermodynamic Cycle of the Eskom AHTR.

Wright, G., et al. (2015). "Silicon Carbide as a tritium permeation barrier in tungsten plasma-facing components." Journal of Nuclear Materials **458**: 272-274.

Zhang, P., et al. (2018). "Evaluation of thermal physical properties of molten nitrate salts with low melting temperature." Solar Energy Materials and Solar Cells **176**: 36-41.

APPENDIX A (EES SCOPING CODE)

```
"Inputs"

T_salt_in = 480.629

T_salt_out = 517.303

T_helium_in = 630

T_helium_out = 510.766

m_dot_helium = 24.092

m_dot_salt = 244.765

enthalphy_He_in = 4702.433

enthalphy_He_out = 4083.317

enthalphy_salt_in = 1150.243

enthalphy_salt_out = 1210.955

pressure_helium_in = 2369.154

pressure_helium_out = 2345.697

pressure_drop_helium = 23457 [Pa]

"Scoping calculations"

Heat_duty = m_dot_helium*(enthalphy_He_in-enthalphy_He_out)

C_helium = Heat_duty/(T_helium_in-T_helium_out)

C_salt = Heat_duty/(T_salt_out-T_salt_in)

C_star = C_helium/C_salt

effectiveness = (C_helium*(T_helium_in-T_helium_out))/(C_helium*(T_helium_in-T_salt_in))

NTU = (1/(C_star-1))*ln((effectiveness-1)/(C_star*effectiveness-1))

N_helium = 1.1*NTU

N_salt = 1/((C_salt/C_helium)*((1/NTU)-(1/(N_helium))))

j = 0.25

T_mean_salt = (T_salt_out+T_salt_in)/2

T_mean_helium = (T_helium_in+T_helium_out)/2

P_mean_helium = (pressure_helium_in +pressure_helium_out)/2
```

P_mean_salt = 101.3

Cp_helium =Cp(Helium,T=T_mean_helium,P=P_mean_helium)

Cp_salt = 1.62

Viscosity_helium = Viscosity(Helium,T=T_mean_helium,P=P_mean_helium)

Viscosity_salt = 0.002

Conduction_helium =Conductivity(Helium,T=T_mean_helium,P=P_mean_helium)

Conduction_salt = 0.5

rho_helium =Density(Helium,T=T_mean_helium,P=P_mean_helium)

rho_salt = (2.346-0.000765*(273.15+T_mean_salt))*1000

Pr_helium =Prandtl(Helium,T=T_mean_helium,P=P_mean_helium)

Pr_salt = ((Cp_salt*Viscosity_salt)/Conduction_salt)*1000

G_helium = sqrt((2*rho_helium*pressure_drop_helium*j)/(N_helium*Pr_helium))

G_salt = sqrt((2*rho_salt*50000*j)/(N_salt*Pr_salt))

Flow_area_helium = m_dot_helium/G_helium

Flow_area_salt = m_dot_salt/G_salt

Velocity_flow_helium = m_dot_helium/(rho_helium*Flow_area_helium)

Velocity_flow_salt = m_dot_salt/(rho_salt*Flow_area_salt)

d_helium = 0.001

dh_helium = d_helium/(1+2/pi)

d_salt = d_helium

dh_salt = d_salt/(1+2/pi)

Re_helium = (rho_helium*Velocity_flow_helium*dh_helium)/Viscosity_helium

Re_salt = (rho_salt*Velocity_flow_salt*dh_salt)/Viscosity_salt

Nu_helium = 0.023*Re_helium^(4/5)*Pr_helium^0.3

Nu_salt = 4.36

L_helium = (Pr_helium*Re_helium*dh_helium*N_helium)/(4*Nu_helium)

L_salt = (Pr_salt*Re_salt*dh_salt*N_salt)/(4*Nu_salt)